Chemical Science

ROYAL SOCIETY OF CHEMISTRY

REVIEW

View Article Online
View Journal | View Issue

Cite this: *Chem. Sci.*, 2022, **13**, 611

Chiral assembly of organic luminogens with aggregation-induced emission

Chenchen Liu,†[a] Jun-Cheng Yang,†[b] Jacky W. Y. Lam,[a] Hai-Tao Feng *[b] and Ben Zhong Tang *[acdef]

Chirality is important to chemistry, biology and optoelectronic materials. The study on chirality has lasted for more than 170 years since its discovery. Recently, chiral materials with aggregation-induced emission (AIE) have attracted increasing interest because of their fascinating photophysical properties. In this review, we discussed the recent development of chiral materials with AIE properties, including their molecular structures, self-assembly and functions. Generally, the most effective strategy to design a chiral AIE luminogen (AIEgen) is to attach a chiral scaffold to an AIE-active fluorophore through covalent bonds. Moreover, some propeller-like or shell-like AIEgens without chiral units exhibit latent chirality upon mirror image symmetry breaking. The chirality of achiral AIEgens can also be induced by some optically active molecules through non-covalent interactions. The introduction of an AIE unit into chiral materials can enhance the efficiency of their circularly polarized luminescence (CPL) in the solid state and the dissymmetric factors of their helical architectures formed through self-assembly. Thus, highly efficient circularly polarized organic light-emitting diodes (CPOLEDs) with AIE characteristics are developed and show great potential in 3D displays. Chiral AIEgens are also widely utilized as "turn on" sensors for rapid enantioselective determination of chiral reagents. It is anticipated that the present review can entice readers to realize the importance of chirality and attract much more chemists to contribute their efforts to chirality and AIE study.

Received 26th April 2021
Accepted 24th May 2021

DOI: 10.1039/d1sc02305e

rsc.li/chemical-science

1. Introduction

Chirality is a universal phenomenon in nature and refers to molecules, objects and materials that are non-superimposable on their mirror images. As an essential feature of life, the research of chirality has drawn enormous attention not only in chemistry, biology and physics, but also in astronomy and architecture at different dimensions and scales.[1] In other words, the building blocks of life are chiral. For example, proteins are composed of only left-handed amino acids, and spiral galaxies rotate in one direction. Why our life and world are chiral? This puzzles scientists for generations and drives people to investigate the chiral phenomenon and materials.[2–4] In addition, more than half of commercial drugs are chiral compounds and must be separated into pure enantiomers.[5] They often possess different physiological toxicity. For example, *R*-thalidomide has been used against nausea and alleviates morning sickness in pregnant women. However, its *S*-enantiomer causes severe phocomelia.[6] As a result, modern drugs must be accurately determined before clinical use. Taking this into account, enantiorecognition and raceme resolution are the hotspots in pharmaceutical analysis, food chemistry and life science.[7–9] To date, several techniques have been employed to separate and discriminate enantiomers including high-performance liquid chromatography (HPLC), nuclear magnetic resonance, UV/vis, circular dichroism (CD), and fluorescence spectroscopy.[10–13] For example, CD spectroscopy is a powerful tool for the detection of receptor–analyte interactions where CD-silent probes can be activated or the signals of CD-active probes can be modulated, and it can also be used orthogonally to other spectroscopic techniques.[14–18] In addition, fluorometric techniques have attracted intense interest because of their time-efficiency, high sensitivity, low cost and real-time analysis.[19–22]

[a]*Department of Chemistry, Hong Kong Branch of Chinese National Engineering Research Center for Tissue Restoration and Reconstruction, Institute for Advanced Study and Department of Chemical and Biomedical Engineering, The Hong Kong University of Science and Technology, Clear Water Bay, Kowloon, Hong Kong, China. E-mail: tangbenz@ust.hk*

[b]*AIE Research Center, Shaanxi Key Laboratory of Phytochemistry, College of Chemistry and Chemical Engineering, Baoji University of Arts and Sciences, Baoji 721013, China. E-mail: haitaofeng907@163.com*

[c]*State Key Laboratory of Luminescent Materials and Devices, SCUT-HKUST Joint Research Institute, Center for Aggregation-Induced Emission, China*

[d]*AIE Institute, Guangzhou Development District, Guangzhou, 510530, China*

[e]*Shenzhen Institute of Aggregate Science and Technology, School of Science and Engineering, The Chinese University of Hong Kong, Shenzhen, Guangdong 518172, China*

[f]*Guangdong-Hong Kong-Macau Joint Laboratory of Optoelectronic and Magnetic Functional Materials, China*

† C. L. and J. C. Y. contributed equally to this work.

In recent years, the development of enantioselective fluorescent sensors has been demonstrated to be an efficient method for high throughput screening of chiral catalysts and molecules. For example, Pu reported a series of 1,1′-bi-2-naphthol-based fluorescent sensors to discern chiral amino alcohols, α-hydroxycarboxylic acids, and amino acid derivatives.[22] In addition, due to the development of modern spectroscopic techniques, novel photophysical phenomena are observed in chiral luminogens such as CD and circularly polarized luminescence (CPL).[23] The CD spectrum gives the absorption difference of left- and right-handed CPL in the ground state. It can be quantified by the absorption dissymmetry factor ($g_{abs} = 2(\varepsilon_L - \varepsilon_R)/(\varepsilon_L + \varepsilon_R)$), where ε denotes the extinction coefficient of left (L) and right (R) CPL, respectively.[24] CD is mainly utilized to characterize the tertiary structure of proteins and chiral recognition.[13,25] In contrast, CPL is a relatively new research field due to the recent availability of commercial instruments, the measurement of CPL affords the emission difference of left- and right-handed CPL in the excited state.[26] The CPL performance is evaluated by the emission dissymmetry factor (g_{em}), which is defined as $g_{em} = 2(I_L - I_R)/(I_L + I_R)$ and indicates the degree of preference of one type of CPL over the other. For both CD and CPL, a large g value is a primary criterion to appraise the chiroptical properties of a fluorophore.

To date, the emission of most reported chiral fluorescent materials are studied in solution.[20,21] When these molecules are aggregated in a poor solvent, their emission is weakened or even completely annihilated because of the aggregation-caused quenching (ACQ) effect (Fig. 1A).[27] This dramatically affects their CPL performance and chiral recognition. Recently, some organic fluorophores with molecular rotors, such as hexaphenylsilole (HPS),[28] tetraphenylethene (TPE)[29–31] and α-phenylcinnamonitrile,[32,33] have fluoresced weakly in the solution state, but emitted intensely in aggregates or the solid state (Fig. 1B). This phenomenon is termed aggregation-induced emission (AIE) and is caused by the restriction of intramolecular motion (RIM) including intramolecular rotation and vibration.[28,34] Such a mechanism is supported by cogent experiments and theoretical analysis,[35–37] and it states that in the solution state, the excited-state energy of AIE luminogens (AIEgens) is consumed by molecular rotation and vibration. However, in the aggregate state, these motions are hampered to activate radiative transition, which makes the luminogens emissive.[38] Now, using AIEgens has been recognized as a promising protocol to design new chiral fluorophores. The resulting AIEgens can often effectively impede fluorescence quenching and enhance the CPL efficiency in the condensed state.[39] Interestingly, some propeller-like or shell-like AIEgens without chiral units exhibit latent chirality upon mirror image symmetry breaking.[40–42] In addition, some optically active molecules can transfer the chirality to achiral AIEgens by non-covalent interactions.[43–46] Thus, a simple and convenient strategy to achieve CPL has been developed by the co-assembly of achiral AIEgens and chiral materials.

Herein, this review summarized the molecular structures of chiral AIEgens and prochiral AIEgens and the chiral induction of achiral AIEgens. Attention is also given to supramolecular assembly, which is beneficial for chiral materials to achieve high emission efficiency and dissymmetry factors in the aggregate state. The CD/CPL of chiral AIE materials will be discussed and their applications in circularly polarized organic light-emitting diodes (CPOLEDs) and chiral recognition will be presented as well.

2. Molecular structures

2.1 Chiral AIEgens

The modification of AIEgens with chiral groups is a widely adopted strategy to construct chiral AIEgens. In this section, we focused on the molecular structures of recently reported chiral AIEgens. Among them, 1-methyl-1,2,3,4,5-pentaphenyl-silole and TPE as two classical AIEgens have been popularly utilized. In addition, some other chiral AIEgens based on cyanostilbene and 1,1′-bi-2-naphthol (BINOL) were introduced.

2.1.1 Silole-cored chiral AIEgens. As the first AIE example, silole is well-known for its high fluorescence efficiency and

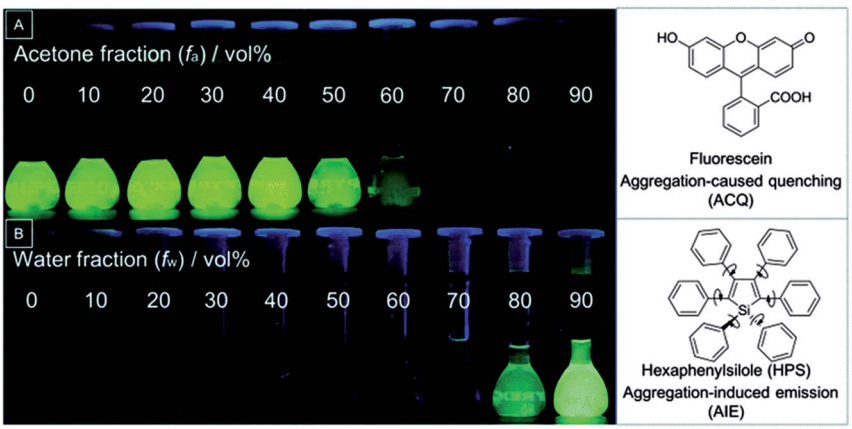

Fig. 1 Fluorescence images of (A) fluorescein (1.5×10^{-2} M) in a mixed solvent of water and acetone with different fractions of acetone (f_a), and (B) hexaphenylsilole (HPS; 1.0×10^{-2} M) in a mixed solvent of THF and water with different fractions of water (f_w). Reproduced from ref. 34 with permission. Copyright 2015 the Royal Society of Chemistry.

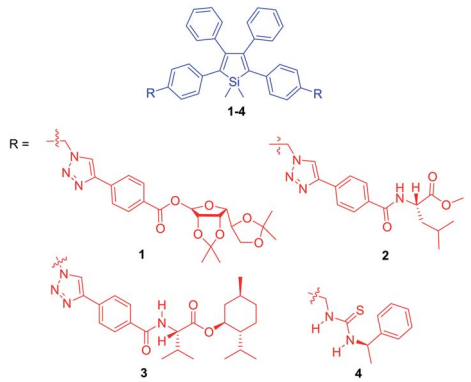

Fig. 2 Molecular structures of silole-based chiral AIEgens.

photostability.[28] Thus, many silole-based AIEgens have been successfully designed and synthesized for sensors, optoelectronic devices and so on.[47] It is also anticipated that silole-based AIEgens are promising scaffolds to construct chiral light-emitting materials. Recently, a series of silole-based chiral molecules **1–4** with AIE characteristics were reported by Tang (Fig. 2). Molecule **1** was synthesized by the incorporation of a mannose unit into the tetraphenylsilole backbone through a "click" reaction.[48] By using a similar synthetic method, Tang prepared two other chiral AIEgens **2** and **3** with L-valine and L-leucine pendants, respectively.[49,50] To enlarge the molecule library, AIEgen **4** was then designed by introducing a chiral phenylethanamine unit into the tetraphenylsilole skeleton through thiourea tether.[51] These silole derivatives all showed obvious AIE characteristics.

2.1.2 TPE-cored chiral AIEgens. As the first generation of AIEgens, silole derivatives possess high quantum yields. However, their preparation is quite complicated. Thus, TPE, another star AIEgen, is widely applied to construct various chiral materials due to its facile synthesis, high emission efficiency and excellent chemical stability (Fig. 3). For example, Tang synthesized a chiral TPE derivative **5** bearing an L-leucine methyl ester moiety, which was CD-active and showed strong CPL in the aggregate state.[52] Zheng reported a couple of chiral TPE derivatives **6** with (1*S*,2*R*)/(1*R*,2*S*)-**1**, 2-diphenyl-2-aminoethanol as a chiral receptor.[53] By virtue of acid–base interaction and hydrogen bonding, compound **6** was used as a chiral sensor to discriminate a large number of chiral acids with high enantioselectivity and high sensitivity. To widen the analyte scope for chiral recognition, TPE macrocycle **7** with the AIE effect was synthesized by tethering an optically pure diphenyldiaminoethylene group.[54] It is anticipated that the additional cavity of the macrocycle may enhance its selectivity for analytes.[55,56] The results showed that this compound could discriminate a series of chiral acids and α-amino acids by enantioselective aggregation and the AIE effect. Two naphthalenediimide-TPE derivatives were synthesized by Bhosale, and the chiral alanine spacers induced the formation of left- and right-handed twisted ribbons based on solvophobic control.[57] To visualize the chiral amplification process in liquid crystals (LCs), a chiral TPE derivative **8** with cholesterol periphery was prepared through an acylation reaction.[58] This chiral AIE molecule could form helical assemblies with empty space in the aggregate state and enable the co-assembly of LCs with the helical templates to form structures with a similar

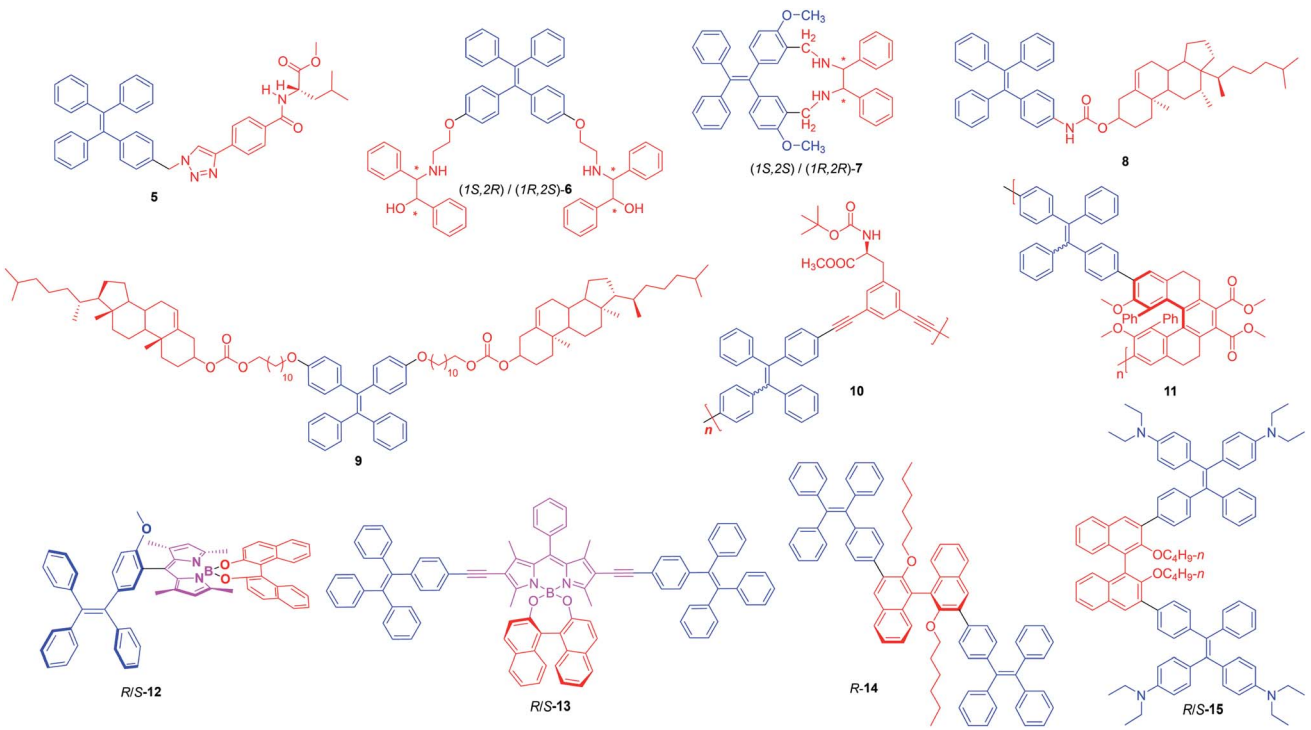

Fig. 3 Molecular structures of TPE-based chiral AIEgens.

helical arrangement and a morphology of pearled necklaces or thick rods. Meanwhile, the CD and CPL signals were significantly amplified during the host-guest assembly. Lu also synthesized a TPE derivative **9** bearing cholesterol pendants, which displayed typical AIE and liquid crystalline properties.[59] The AIE molecules showed helical orientation in LCs to result in a huge difference in left and right CPL emissions, and the CD and CPL behaviors were found to be strongly influenced by the change of temperature.

Chiral polymers have attracted increasing interest due to their great potential applications in enantioselective recognition, CPL, asymmetric catalysis and so on.[60] Thus, Cheng synthesized a TPE-based polymer **10** bearing an L-tyrosine derivative in the side-chain.[61] Polymer **10** showed weak emission in THF solution. However, upon aggregation in water, enhanced green fluorescence and CPL intensity were gradually observed. However, the g_{em} value decreased due to the weakening of the chiral signals caused by the extrinsic heterogeneities of aggregates. Therefore, the isolated molecules in THF solution could generate a high g_{em} value in this system. Based on helical aromatic esters, Chen designed a new kind of AIE-active chiral polymer **11**,[62] which showed typical aggregation-induced CPL (AICPL) in a THF and water mixture. Mirror-imaged CD spectra were obtained in both solution and aggregates, and uniform nanospheres were formed in the THF/water (2 : 8, v/v) mixture. These nanostructures assembled from **11** also exhibited obvious CPL with a g_{em} value of 1.04×10^{-3}.

Unlike the above mentioned AIEgens with point chirality, compounds **12–15** formed by the attachment of BINOL to the TPE scaffold showed axial chirality. The TPE-BINOL derivatives *R*/*S*-**12** were reported by Feng.[63] These molecules emitted strong green fluorescence in THF solution, which red-shifted to the yellow region upon aggregate formation by the addition of water. *R*/*S*-**12** showed good mirror CD bands with a monosignate band at 340 nm and 507 nm in THF, and upon addition of a 95% water fraction, the absorption band red-shifted to 522 nm with enhanced intensity. Cheng reported a set of red-emitting enantiomers *R*/*S*-**13** with TPE, BINOL and BODIPY,[64] which were CD-active in both solution and condensed phases. The CPL bands showed little variance in different dichloromethane/hexane mixtures, indicating that their chiroptical properties were independent of aggregation. Unlike most chiral AIEgens, compound **14** exhibited an abnormal phenomenon of aggregation-annihilation CD.[65] The CD signals remained unchanged in THF solution and THF/water mixtures with a water fraction of up to 40%. Upon further enhancement of the water fraction, the CD intensity, however, was sharply decreased probably due to the decrease of the twisting angle between the two naphthalene rings in the aggregate state. Other binaphthyl derivatives *R*/*S*-**15** were successfully designed and showed no CPL signals in THF.[66] Interestingly, obvious mirror-imaged CPL bands were observed in their spin-coated films with a g_{em} value of 2.8×10^{-3}, indicative of a typical AICPL characteristic. *R*/*S*-**15** was successfully applied for fabricating CPOLEDs with a low turn-on voltage of 3.18 V, a high maximum brightness of 8061 cd m^{-2} and a low external quantum yield of 0.48%.

2.1.3 Other chiral AIEgens. Apart from silole and TPE-cored chiral AIEgens, many chiral AIEgens based on BINOL, metal complexes and cyanostilbene were reported (Fig. 4). For example, the dynamic self-assembly process of AIE-active chiral Au(I) complexes **16** was visualized by their morphological change from vesicles to helical fibers, and the helical nanostructures could co-assemble with achiral luminogens to induce CPL.[67] On the other hand, a series of chiral AIEgens **17–20** were synthesized by melding binaphthyl moieties with carbazole units, which were ideal chiral emitting materials with delayed fluorescence for fabricating efficient CPOLEDs.[68] In addition, chiral AIEgen **21** with maximized chiral perturbation efficiency was rationally designed and was used to fabricate top-emissive CPOLEDs with high performance.[69] Zang reported a pair of photo-responsive chiral AIE Cu(I) clusters **22** based on BINOL showing bright luminescence by virtue of their metal cluster and triplet metal-to-ligand charge-transfer.[70] Moreover, the good ability of the chiral Cu(I) clusters to generate reactive oxygen species made them promising for photodynamic therapy. Zang also prepared another pair of chiral ligands **23** for synthesizing copper(I) alkynyl clusters with unique AIE and crystallization-induced emission.[71] The clusters exhibited good CPL performance and were further exploited for bioimaging with good biocompatibility. Haino, on the other hand, reported several chiral Pt(II) phenylbipyridine complexes **24** showing aggregation enhanced emission.[72,73] **24A** was CD silent and showed non-helical assemblies in chloroform. When the solvent was changed to toluene, obvious helical assemblies with enhanced positive Cotton effects were gradually generated. Its analogue **24B** with long side-chains and chiral alkyl chains was molecularly dissolved in 1-decanol and showed no CD signals at 50 °C. When the temperature was decreased to 10 °C, sol-to-gel transition occurred, which induced obvious CD and CPL signals with a g_{em} value of 0.011. The chiral compound **25** bearing a couple of L-Asp–L-Phe and D-Asp–D-Phe dipeptide sequences was synthesized to prepare supramolecular gels.[74] The nanobelts assembled from L,L-**25** exhibited coiled superhelix nanostructures with an average thickness of 5 nm. However, D,D-**25** could self-assemble into an amazing loop-like nanostructure with a diameter of 9 μm and an average thickness of 140 nm. Such loop-like nanostructures may originate from "layer-by-layer" periodic stacking. A switchable CPL system based on chiral [3]rotaxanes **26** was developed by Yang.[75] The addition or removal of acetate anions can control the movement of the chiral pillar[5]arene macrocycles along the axle to result in switching between two emissions with high photoluminescence quantum yields (PLQYs) and g_{em} values. Jiang realized multi-color tunable CPL in a single AIE molecule by attaching pyridine-modified cyanostilbene to a chiral unit **27**.[76] Due to the chirality transfer and amplification by gelation, the molecule formed gel and xerogel films with blue CPL and a large g_{em} value. The CPL signals of the xerogel films red-shifted when the pyridine group was protonated to realize multi-color CPL emission from blue to orange. On the other hand, Zheng synthesized chiral AIE sensors D/L-**28A** by attaching tartaric acid to the 2-phenylcinnamylnitrile backbone, which served as chiral

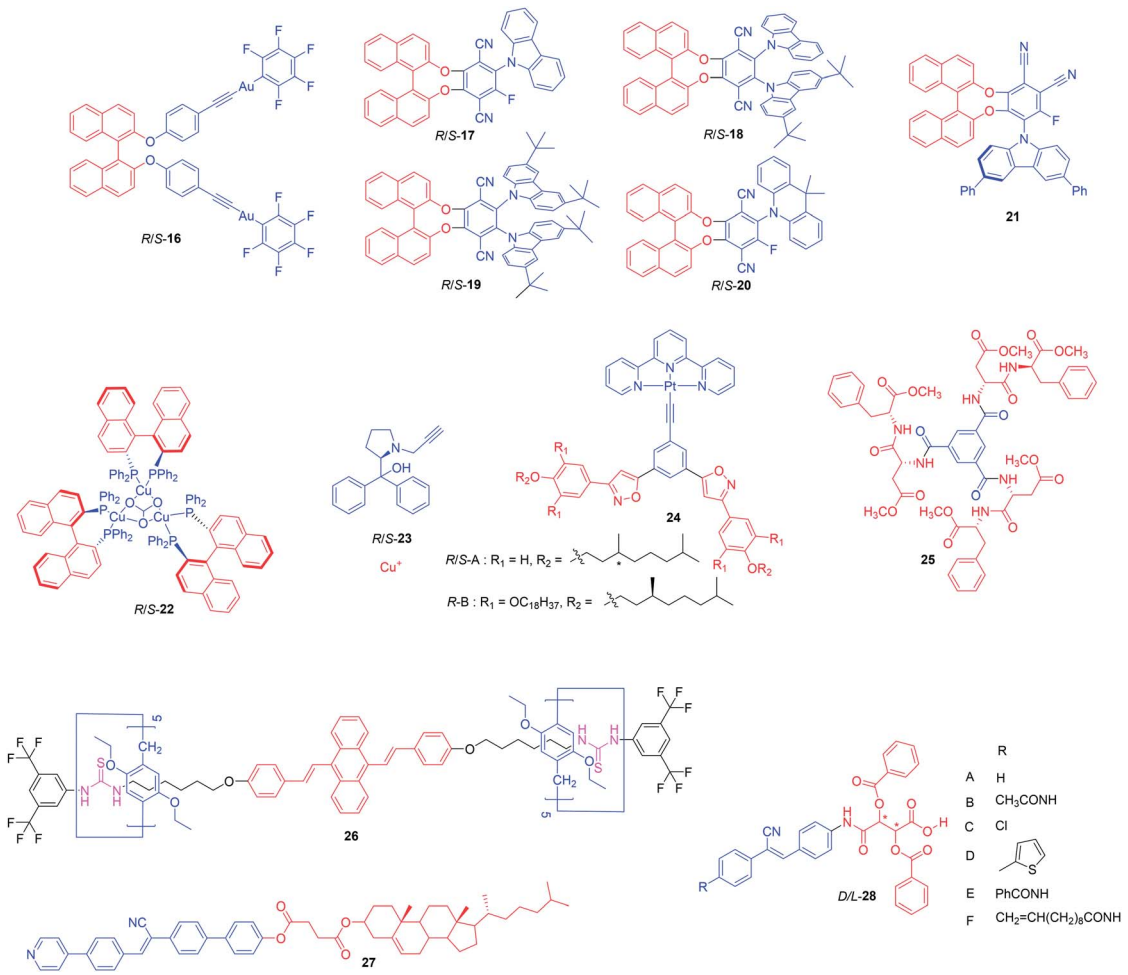

Fig. 4 Molecular structures of other chiral AIEgens.

"turn-on" sensors to form aggregates with enantiomers. Based on the acid–base interaction, D/L-**28A** was used to discriminate a set of chiral amines.[77,78]

2.2 Prochiral AIEgens

Some AIEgens with molecular rotors or vibrators often exhibited intrinsic chirality (Fig. 5). For example, the four phenyl rings of TPE could rotate either in the clockwise or the anticlockwise direction. Thus, no chirality was observed in the solution state due to the rapid and reversible configurational change. However, chirality could be achieved upon aggregation to break the mirror symmetry. For example, the Zhang group mixed three TPE-based derivatives **29–31** with KBr pellets to analyze their solid-state CD spectra.[40] As expected, these molecules exhibited no chirality in solution due to the fast rotations of the phenyl rings. However, in the solid state, the raceme could be separated by mirror symmetry breaking to give the *P*- or *M*-helicity of TPE. To immobilize the propeller-like conformation of TPE in the solution state, Zheng synthesized a TPE-based tetracycle **32** by the lockage of the phenyl rings of TPE through covalent bond connection and resolved the racemic **32** into a set of enantiomers by chiral HPLC.[79] Due to restriction of molecular rotation, *M*/*P*-**32** and racemic **32** fluoresced strongly in THF solution with very high fluorescence quantum yields. Moreover, obvious CPL signals of *M*-**32** and *P*-**32** with mirror images were detected in THF solution and suspension at about 505 nm. Later, the Zheng group developed enantiomers of two other helical TPE tetracycle tetramines *M*/*P*-**33**,[80] and their CPL signals could increase by more than 60-fold after self-assembly into superhelices. Surprisingly, upon addition of one enantiomer of tartaric acid (TA), the self-assembled superhelices could further assemble into longer and wider bundles to generate more than 200-fold CPL enhancement with a very high g_{em} of up to 0.61. The additional assembly also realized exceptional discrimination of TA enantiomers through CPL analysis. By a reversible covalent reaction, a cubic cage **34** bearing six TPE units perched on each face and eight triaminoethylamine units standing the eight vertices of the cube was prepared by Cao.[81] The cage (6*M*)-**34** possessed a cavity of about 11.5 × 11.5 × 11.5 Å^3, which was large enough to encapsulate many guest molecules. Due to the immobilization of free rotation of the TPE unit, strong fluorescence was also observed in dilute solution. In addition, (6*M*)-**34** and (6*P*)-**34** exhibited mirror-imaged

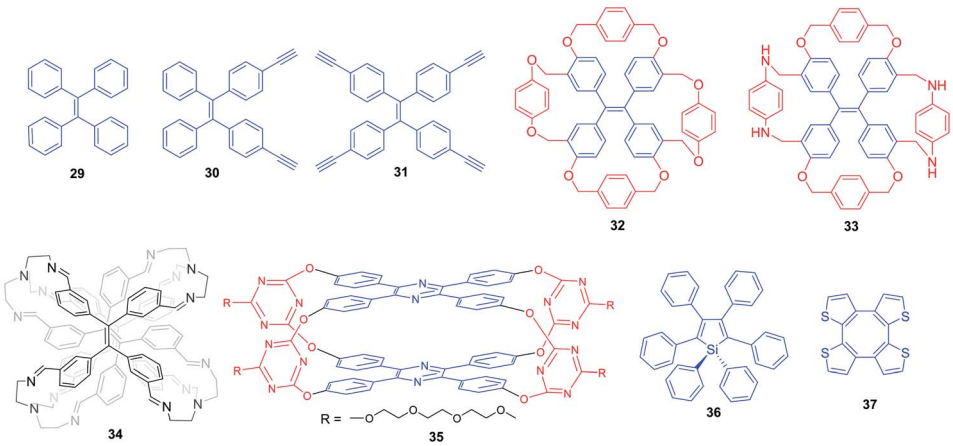

Fig. 5 Molecular structures of prochiral AIEgens.

Cotton effects. Another amphiphilic tetraphenylpyrazine (TPP)-based cage **35** was facilely synthesized by the immobilization of a propeller-like TPP molecule.[82] TPP-Cage **35** showed obvious Cotton effects in the corresponding absorption regions in both solution and nanoparticles, indicating that a chiral TPP-cage was constructed from achiral AIEgens. HPS **36** was another typical prochiral AIEgen, whose chirality could be induced when its six phenyl rings were fixed in a preferred clockwise or anti-clockwise direction in the aggregate state.[41] It could self-assemble into helical nanofibers and nanotubes showing obvious CD and CPL signals. Similarly, some shell-like AIEgens manifested latent chiral characteristics and they could form asymmetrical nanostructures when their intramolecular motions were restricted in the aggregate state. The non-aromatic annulene derivative of cyclooctatetrathiophene **37** was developed by Tang,[42] and the aromaticity reversal from the ground state to the excited state could induce excited-state intramolecular vibration, which provided a new strategy to

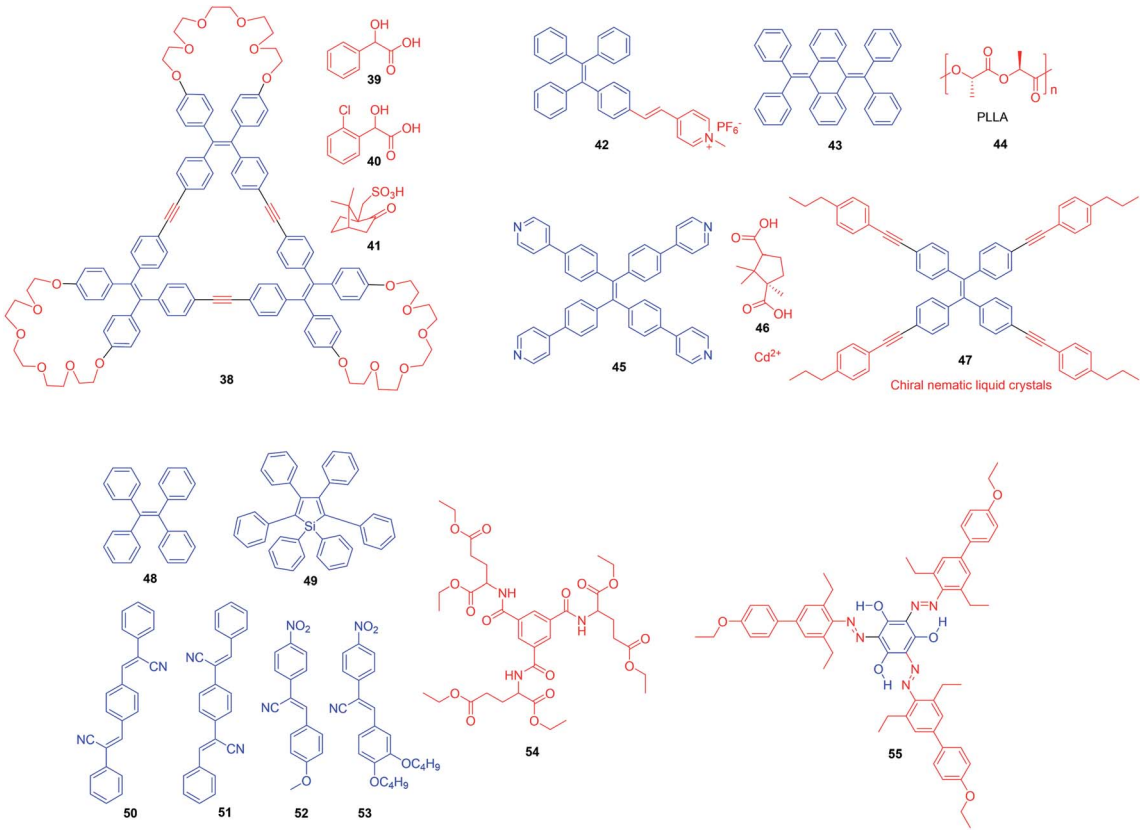

Fig. 6 Molecular structures of achiral AIEgens obtained through chiral induction.

design vibrational AIEgens. The enantiomers of **37** were separated by preparative chiral HPLC and showed strong CD signals in both solution and solid states. In addition, obvious CPL signals were detected in the solid state.

2.3 Chiral induction of achiral AIEgens

Chirality induction by chiral guest molecules or solvents is an efficient method to endow AIEgens with chiroptical properties.[83,84] Recently, Zheng reported a novel triangular macrocycle **38** without chiral signals (Fig. 6).[85] Although partial phenyl rings of the TPE skeleton were fixed by three ethynylene bridging linkers, compound **38** still exhibited typical AIE characteristics because other phenyl rings could still undergo free rotation or vibration in solution. Upon addition of chiral acids **39–41** to the macrocycle film, obvious CD and CPL signals were detected. This result demonstrated that the co-assembly of achiral AIEgens into helical structures was a simple and convenient strategy to achieve CPL. Tang reported a polymorphism-dependent AIEgen **42** with a donor (D)–acceptor (A) structure, which could visualize the amorphous and crystalline phase distribution of poly(L-lactide) (PLLA) **44**.[43] The CPL signal was obtained from the chiral structured spherulites of the AIE-embedded polymer film; meanwhile, the CPL signals could inverse upon flipping the polymeric film. Similarly, tunable emission and white CPL could be generated by embedding a butterfly-shaped AIEgen **43** with polymorphism-dependent emission into the PLLA **44** film.[44] In addition, Liu designed optically pure metal–organic frameworks (MOFs) with AIE characteristics through chiral reticular self-assembly of achiral AIEgen **45** and chiral camphoric acid **46** with Cd^{II} ions.[86] Strong CPL was obtained from the MOF by through-space chirality transfer; moreover, the fluorescence and CPL signals were switchable under reversible external mechano-stimuli like ultrasonication. The chirality of AIEgen **47** could also be induced by chiral nematic liquid crystals, making it suitable to fabricate a CPL-active liquid crystalline display.[87] Chiral C_3 symmetrical molecule **54** could facilely form gel showing hexagonal nanotubes in a wide range of solvents. Based on this result, the Liu group designed a full-color tunable CPL supramolecular system by the encapsulation of AIEgens **48–53** in their cavities because the chirality could transfer from the as-prepared gels to guest AIEgens upon gelation.[45] The supramolecular assembly of an achiral trigonal molecule **55** in different solvents was studied.[88] Helical nanostructures with an equal

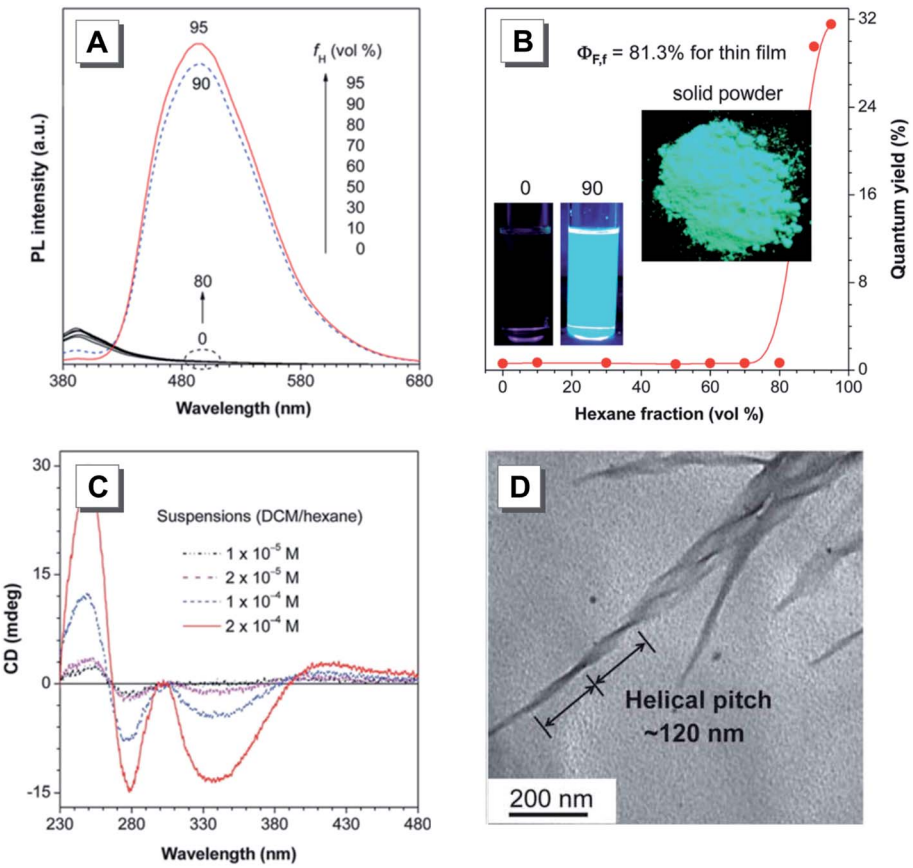

Fig. 7 (A) PL spectra of **1** in a mixed solvent of dichloromethane and hexane with different volume fractions (f_H) of hexane ([**1**] = 1.0×10^{-5} M). (B) Change of fluorescence quantum yields of 1 in different f_H. Insets: Fluorescence photos of **1** in dichloromethane and a mixture of dichloromethane and hexane with 90% hexane, and its powder under irradiation of a 365 nm UV lamp. (C) CD spectra of **1** with different concentrations in DCM/hexane (v/v, 1/9) mixtures. (D) TEM pictures of aggregates of **1** formed in a DCM/hexane mixture (v/v, 1/9). Adapted from ref. 48 with permission. Copyright 2012 the Royal Society of Chemistry.

probability of left- and right-handed helices were attained in a dimethylformamide/H_2O mixture and were also found to show aggregation-induced emission enhancement.

3. Self-assembly

The aggregation of AIEgens during the supramolecular assembly can amplify the CPL signals and the dissymmetry factor. The defined morphology and formation process provide us with more detailed information to understand the mechanism of chiral self-assembly. Tang first reported silole-cored chiral AIEgen **1** by the incorporation of mannose units into a tetraphenylsilole core through an azide–alkyne "click" reaction.[48] The photoluminescence (PL) of **1** was barely changed until more than 80% of hexane was added into a mixed solvent of dichloromethane (DCM) and hexane. At a hexane fraction > 80%, strong PL was observed (Fig. 7A). More specifically, the dilute solution of **1** in DCM was weakly/non-emissive with a low PLQY of ~0.6%. However, in a mixed solvent of DCM/hexane (v/v = 1/9), remarkably enhanced emission with a much higher PLQY (31.5%) was achieved. In addition, the PLQY of **1** was raised to 81.3% in the solid state (Fig. 7B). Many chiral AIEgens showed stronger CD signals in the aggregate state through self-assembly, and this implied that the AICD was a general phenomenon observed in chiral AIEgens. Compound **1** also displayed no CD signal in DCM even at a high solution concentration. However, obvious CD signals were observed at 249, 278 and 340 nm in a DCM/hexane mixture (v/v = 1/9) when the solution concentration was increased from 2×10^{-5} to 2×10^{-4} M (Fig. 7C). Images from transmission electron microscopy (TEM) disclosed that right-handed helical nanoribbons with an average helical pitch of about 120 nm were formed in the suspension (Fig. 7D). The driving force underlying this self-assembly may be attributed to multiple hydrogen-bonding interactions, π–π stacking, and stereo-configuration complementarity between the sugar pendants.

Liquid crystals exhibit remarkable chiral amplification by virtue of their outstanding sensitivity to chiral perturbations.[89–91] However, up to now the mechanisms of chirality transfer and amplification in LCs are still ambiguous. Due to the difficulty in characterizing chirality at different microscales, direct evidence which concerns the schematic model of chiral molecule/LC supramolecular systems is still lacking. Recently, an AIEgen **8** consisting of a TPE scaffold and a chiral cholesterol unit was designed and served as a chiral inducer to co-assemble with 4-cyano-4′-phenylbiphenyl (5CB), a well-known commercial LC, to fabricate a CPL material.[58] Left-handed helical fibers were obtained by twisting thinner elementary fibers of **8** upon evaporation of their THF solution. Moreover, pear-necklace-like architectures with left-handed arrangements were formed when 1 wt% of **8** was doped into 5CB. Both the beads and rods consisting of 5CBs and **8** exhibited an axially oriented arrangement. By further increasing the doping ratio to 2 wt%, beads with a similar helical pitch were also observed and some of them had been coalesced to form helical rods.

The exploration of hierarchical self-assembly processes and the inherent mechanism helps us gain deep insight into the biological helices, materials science, nanotechnology and more. Recently, a chiral BINOL Au(I) complex *R*-**16** exhibiting typical

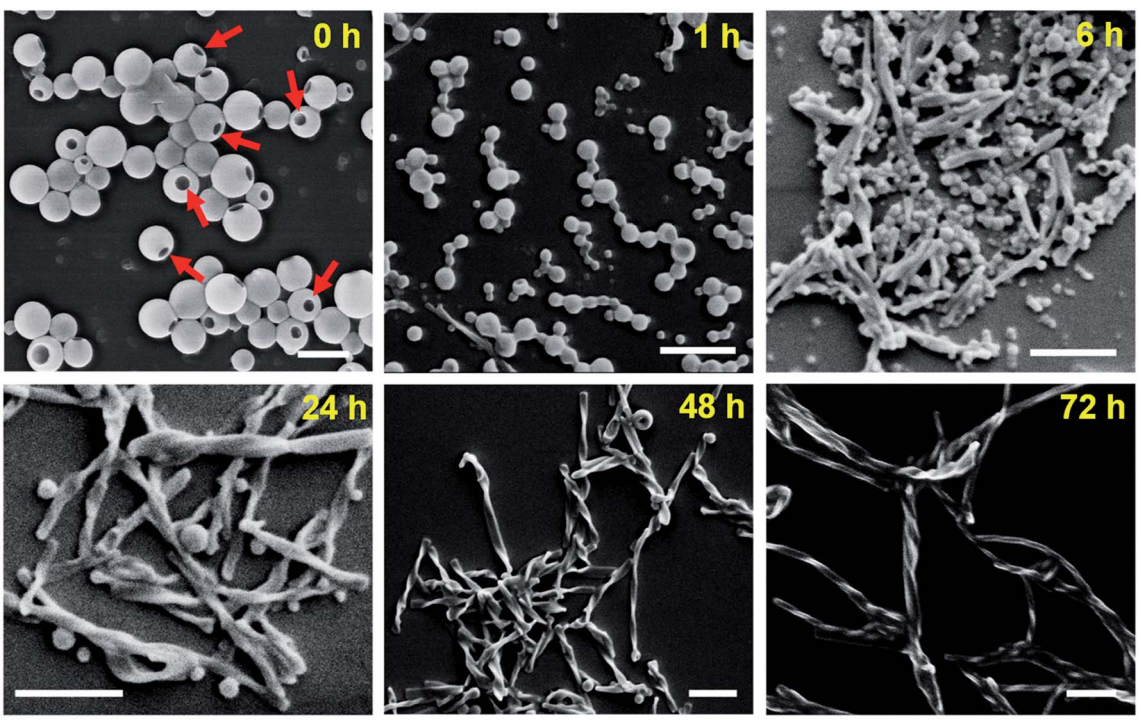

Fig. 8 Time-dependent SEM images to visualize the self-assembly processes of *R*-**16** (THF/water: 1/4, v/v). Scale bar: 500 nm. Adapted from ref. 67 with permission. Copyright 2019 American Chemical Society.

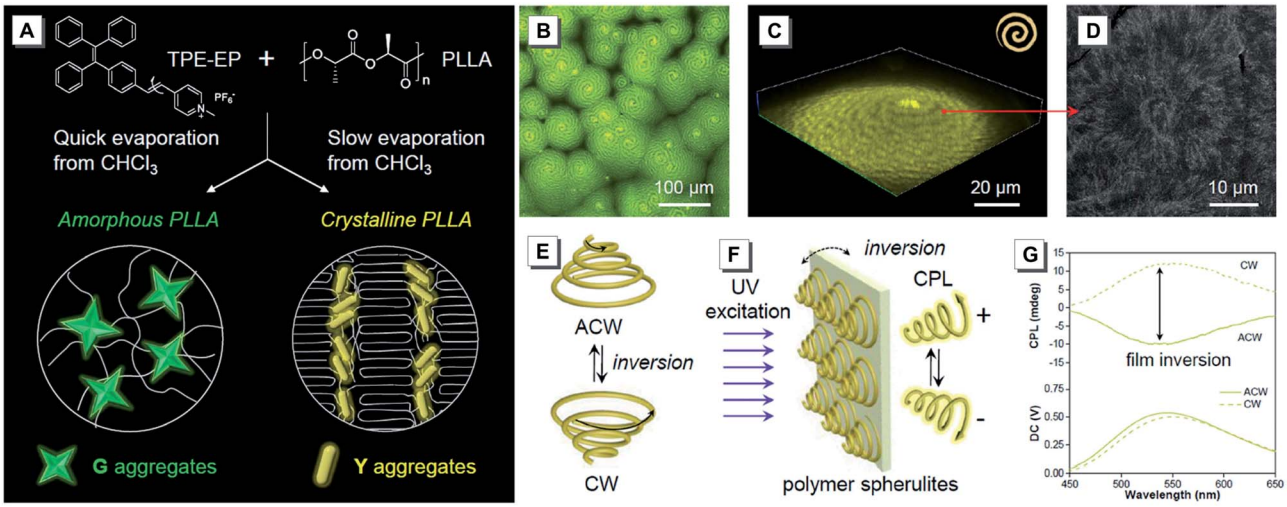

Fig. 9 (A) Preparation of amorphous and crystalline PLLA embedded with **42**. (B) Fluorescence image (2D) and (C) confocal image (3D) of the prepared spherulites with alternative bright and dark yellow spirals in the anticlockwise direction. (D) SEM image of the interior morphological structure in the spherulite etched with acetone. (E) Enantiomeric chirality switching of the spiral spherulites by film inversion. (F) The generation of CPL from a crystalline polymer film and (G) the enantiomeric CPL switching upon film inversion. Adapted from ref. 43 with permission. Copyright 2020 the Royal Society of Chemistry.

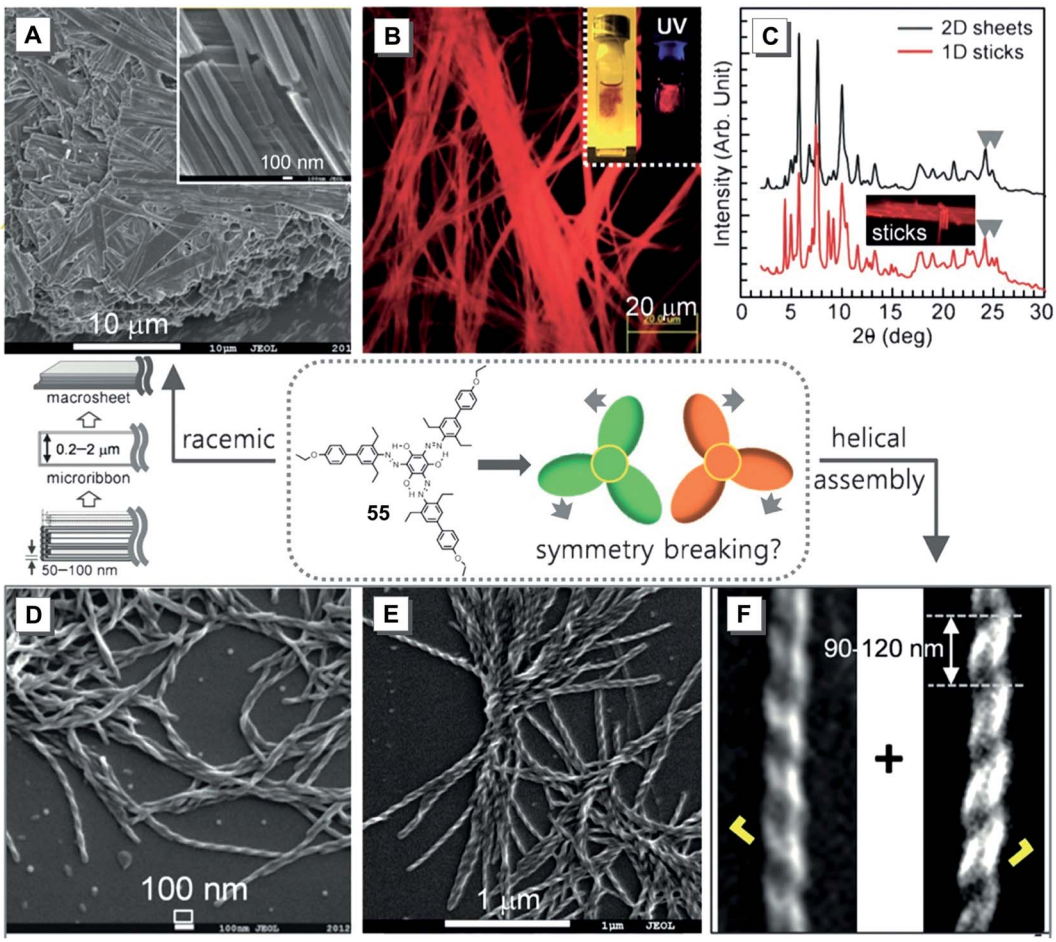

Fig. 10 (A) SEM image of **55** assembled into nanosheets in a mixture of toluene and ethanol. (B) Fluorescence photograph of **55** taken under a fluorescence optical microscope. Red fluorescent ribbons are formed from entangled nanoribbons. Inset: Red fluorescent **55** floating nanostructures generated in a mixture of toluene and ethanol. (C) XRD pattern of 2D sheets (black) and 1D sticks (red). (D–F) SEM images of **55** assembled into helical architectures (D) in a DMF/H_2O mixture (v : v, 5 : 1), [**55**] = 1.7×10^{-5} M and (E) in DMF solution, [**55**] = 2.0×10^{-5} M. Adapted from ref. 88 with permission. Copyright 2016 Wiley-VCH.

AIE properties was readily synthesized.[67] As shown in Fig. 8, the time-dependent scanning electrical microscopy (SEM) images of *R*-**16** allowed us to visualize the dynamic self-assembly process on a time scale of hours. The SEM results confirmed the morphological transformation of aggregates from vesicles to helical structures. First, the vesicles were generated by the aggregation of *R*-**16** in newly prepared THF/water solutions. After incubation for 1 h, these vesicles started to adjoin with each other to form necklace-like nanospheres. After 6 h, loosely twisted helical fibers or rods were formed by axial elongation and fusion of nanospheres. After 3 days, left-handed helical nanoribbons were finally formed. In addition, the Au(I) complex could serve as a chiral template to assemble with achiral AIEgens to effectively enhance the CPL signals.

Polymer morphologies are demonstrated to exert a great influence on the properties of materials. Because of the superior sensitivity of AIEgens to their surrounding microenvironment, a few polymer systems with AIE features had been exploited for the spatial visualization of morphologies.[43,44,62] Recently, Tang reported an AIE-based system that could be used as a morphological visualizer for the polymer microenvironment.[43] As shown in Fig. 9A, an amphiphilic AIEgen **42** TPE–EP with a D–A structure was prepared and doped into semi-crystalline PLLA **44**. By fast evaporation of their chloroform solution, an amorphous PLLA film with green fluorescence from thermodynamically stable G aggregates of TPE–EP was obtained and detected. However, a crystalline polymer film was obtained by slow evaporation and metastable Y aggregates of TPE–EP with yellow fluorescence were obtained within the polymer network. At a reasonably slow evaporation rate, the resulting PLLA films showed banded spherulites with alternative bright and dark yellow spirals in the anticlockwise direction (Fig. 9B), which was accomplished by the helical assemblies of PLLA chains. Moreover, the spiral morphology of PLLA spherulites was further confirmed by the fluorescence confocal image and SEM image (Fig. 9C and D). The CPL measurement showed enantiomeric chirality switching of the spiral PLLA spherulites by film inversion, where the spiral spherulites varied from the anticlockwise (ACW) to the clockwise (CW) direction (Fig. 9E–G). Upon UV excitation from frontward and backward sides, opposite CPL signals from the AIEgen-embedded polymer films with chiral spherulites were detected. As a result, a positive CPL

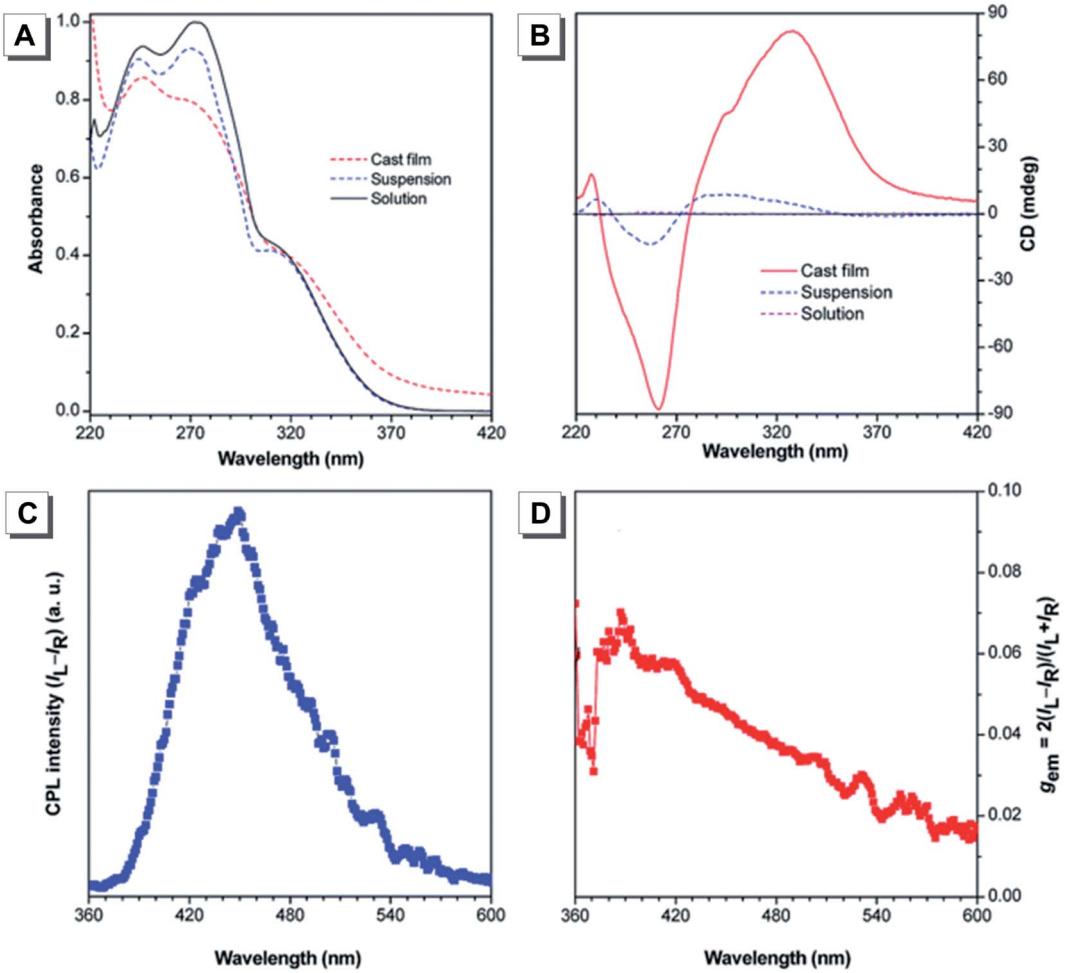

Fig. 11 (A) UV absorption and (B) CD spectra of **5** in 1,2-dichloroethane (DCE) and DCE/hexane (1/9, v/v) suspension, and the cast film state. (C) CPL spectrum and (D) CPL dissymmetry factor g_{em} of **5** prepared by casting its solution on a quartz substrate. Adapted from ref. 52 with permission. Copyright 2015 the Royal Society of Chemistry.

signal from the CW spherulites and a negative CPL signal from the ACW ones were produced, respectively.

Chirality is a central science of life. Research on helical assembly is important for mimicking the double helix of DNA. Because of this purpose, Han and co-workers prepared a series supramolecular structures by using an achiral trigonal molecule **55** in different solvents.[88] Molecule **55** was weakly emissive in toluene. When a poor solvent of ethanol was added in this system, bright red fluorescence was observed. Meanwhile, nanosheets were generated in a mixture of toluene and ethanol (Fig. 10A). After a long-term storage, **55** assembled into red fluorescent microsheets with a width of approximately 0.2–2 μm in mixtures of ethanol and toluene as shown in Fig. 10B. When the solvent was changed to ethyl acetate, ordered sticks were formed (Fig. 10C). Interestingly, the addition of water to a DMF solution of **55** generated structures with an equal probability of left- and right-handed helices (Fig. 10D). The width and pitch length of these helical structures ranged from 30–60 nm and 90–120 nm, respectively (Fig. 10F). Such artificial helical assemblies with the same spin direction were randomly entangled with each other (Fig. 10E), but they failed to assemble into much higher-ordered nanostructures. These elaborated helixes may origin from the self-assembly of achiral molecules with spontaneous symmetry breaking.

4. Functions

4.1 CPL

As mentioned before, CD is a powerful tool to analyze chiral molecules in the ground state, while CPL provides chiroptical information in the excited state. Recently, CPL materials have attracted much more attention in the field of biosensing and optoelectronic devices.[92–94] Conventional CPL materials showed bright fluorescence in solution with absolute g_{em} values of 10^{-5} to 10^{-2}, but their CPL performance dramatically deteriorated in the solid state due to the ACQ effect. In contrast, chiral AIEgens showed weak CPL in solution, but emitted strong fluorescence in the aggregate state with an enhanced g_{em} value. Such a phenomenon was termed AICPL. From the viewpoint of practical applications, chiral materials with aggregation-induced emission are much more promising.[95]

Up to now, thousands of TPE derivatives have been reported including those with chirality and CPL. For example, Tang designed and synthesized a chiral TPE derivative **5** bearing an L-leucine methyl ester moiety.[52] As shown in Fig. 11A, the

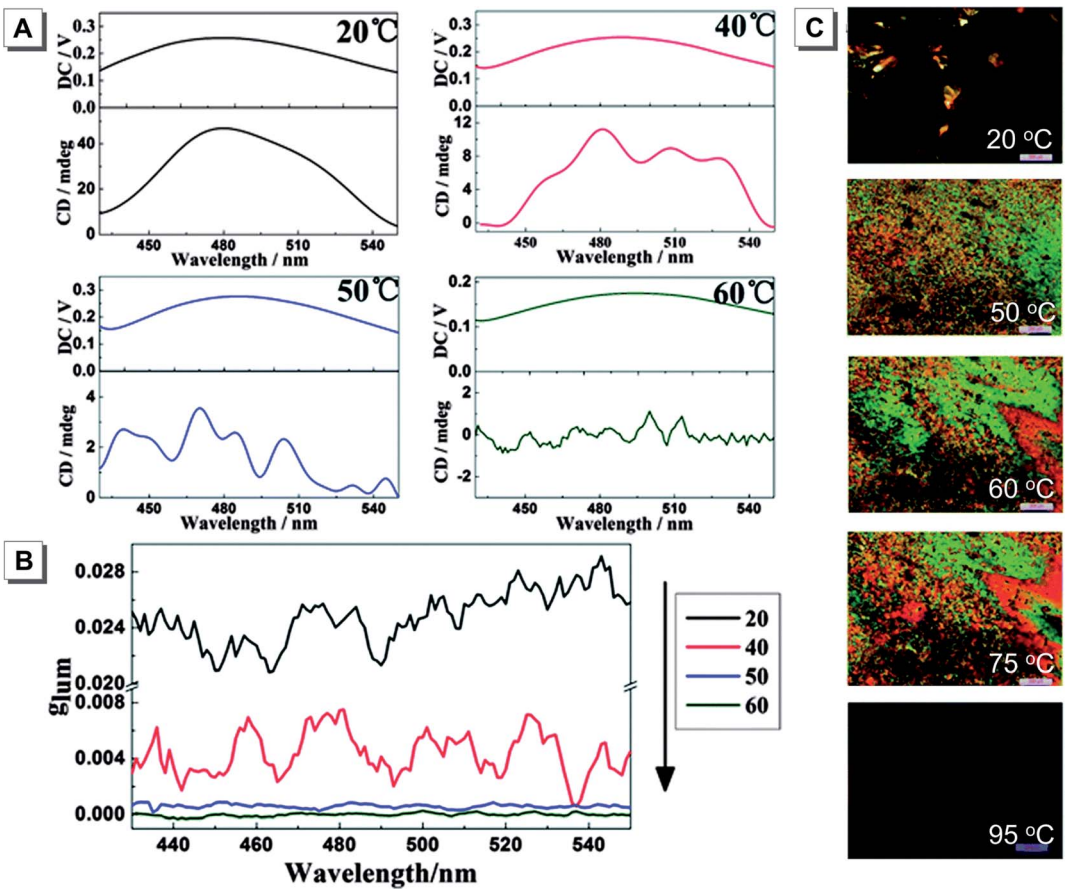

Fig. 12 (A) Luminescence spectra (top), circularly polarized luminescence spectra (bottom) and (B) the corresponding luminescence dissymmetry factors (g_{em}) of **9** cast films treated at different temperatures: 20, 40, 50, and 60 °C. (C) POM photos of **9** at different temperatures: 20, 50, 60, 75 and 95 °C. Scale bar: 200 mm. Adapted from ref. 59 with permission. Copyright 2015 the Royal Society of Chemistry.

absorption peak at ~315 nm corresponded to the absorption of the TPE unit of **5** in solution and aggregated states. Compound **5** was non-emissive and CD silent in solution, but it emitted strong fluorescence and became CD active in the aggregated state (Fig. 11B). Its CPL was investigated in the cast film state and showed a positive signal. The calculated g_{em} value was about +0.07, which was moderate among the reported organic molecules (Fig. 11C and D).

On the other hand, some chemists incorporated AIEgens with liquid crystals to explore the effects of molecular packing and orientation on CPL and g_{em}. For example, Lu synthesized a TPE derivative **9** bearing cholesterol pendants with AIE and liquid crystalline properties.[59] The PL intensity of **9** cast films showed no obvious change in response to temperature in a range from 20 °C to 60 °C. All CPL spectra of the films showed left-handed CPL associated with the *P*-helicity, and the CPL signals and g_{em} values became much weaker when the temperature was increased to 50 °C and above (Fig. 12A and B). Amorphous and crystalline states coexisted at 20 °C. When further increasing the temperature to 50 °C, a typical focal conic texture of the cholesteric LC phase was observed. No obvious changes in the LC texture were observed upon further temperature rise, but at 95 °C, which exceeded the temperature of the isotropic state, the visual field was completely dark and the LC phase completely disappeared (Fig. 12C).

To date, the development of metal clusters with luminescence properties has been limited due to the complexity of the design strategy and underlying mechanism. Thus, a few chiral platinum and coinage metal clusters with AIE have been reported and their luminescence mechanisms still remain elusive.[67,70–73] Consequently, the development of novel luminescent metal clusters is challenging but rewarding to gain insight into the corresponding mechanisms. Zang reported a pair of propeller-shaped chiral trinuclear Cu(I) clusters **22** exhibiting both AIE and CPL.[70] In this work, the carbonate ion acted as a coordination center with three Cu(I) atoms to form a $[Cu_3CO_3]^-$ cluster core. Each BINAP ligand further coordinated with Cu(I) atoms in a bidentate mode to form a propeller-shaped structure. In the molecularly dissolved state, the dynamic intramolecular rotation of the phenyl rings exhausted the excited-state energy to quench the light emission. In the aggregate state, the free rotation of the phenyl rings was largely restricted, which resulted in intense metal cluster-centered (MCC) luminescence (Fig. 13A). Compound **22** showed almost

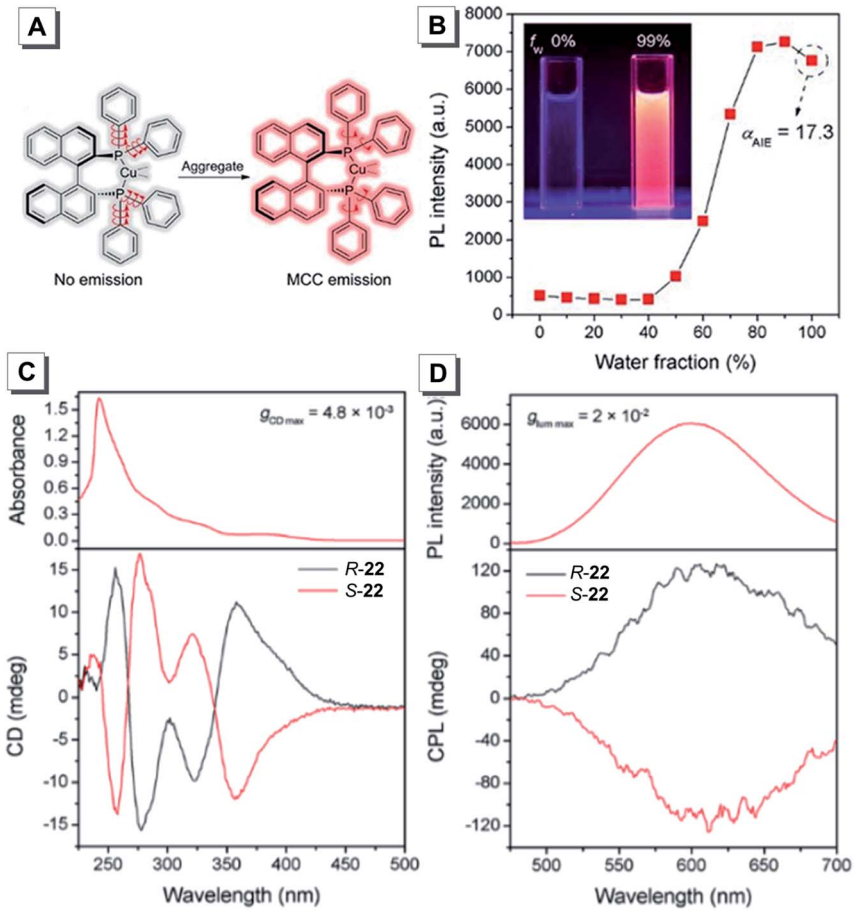

Fig. 13 (A) Schematic program of the RIM mechanism of **22** with metal cluster-centered (MCC) emission. (B) The change of the PL intensity of **22** at 605 nm in DMSO/water mixtures with the increase of the water fraction. (C) Absorption spectra (up) and CD spectra (down) of *R*-**22** and *S*-**22**. (D) Photoluminescence spectra (up) and CPL spectra (down) of *R*-**22** and *S*-**22**. Adapted from ref. 70 with permission. Copyright 2020 Wiley-VCH.

no luminescence in DMSO/H_2O mixtures with a water fraction of less than 40%. Afterwards, the emission intensity rose significantly (Fig. 13B). As shown in Fig. 13C, *R*/*S*-**22** showed clear mirror-imaged CD spectra to reflect the chirality of the Cu(I) clusters. Moreover, obvious CPL signals of *R*-**22** and *S*-**22** with mirror images were detected in aqueous solution at about 610 nm, and the calculated g_{em} values for *R*-**22** and *S*-**22** were 2×10^{-2} and -2×10^{-2}, respectively (Fig. 13D).

The development of multiple switchable CPL systems has shown great potential for application in responsive sensors and smart devices. Recently, a novel CPL switching system based on AIE-active chiral [3]rotaxanes **26** was reported by Yang.[75] As shown in Fig. 14, a typical AIEgen 9,10-distyrylanthracene (DSA) was utilized as a core, thiourea moieties were selected as the binding sites and pillar[5]arene macrocycles (DEP[5]A) were chosen as the stereogenic units and wheel components. In State I, the ethoxy groups of the DEP[5]A wheels formed strong hydrogen-bond interactions with the thiourea units to transfer the chirality of [3]rotaxanes to DSA, to generate CPL with a g_{em} value of 2.14×10^{-3}. The acetate anions showed higher binding affinity to the thiourea moieties and their presence pushed the pillar[5]arene macrocycles to the neutral alkyl chain (State II). Therefore, the chirality information transfer was enhanced and the aggregation behaviors of chiral [3]rotaxanes were influenced to lead to a remarkable enhancement in CPL signals with a g_{em} value of up to 1.36×10^{-2}. Moreover, the addition of Na^+ formed a NaOAc precipitate and removed the acetate anions. Thus, the pillar[5]arene macrocycles and their CPL moved back to State I. This work provides us with a possible approach to design switchable CPL systems for practical applications.

To date, it is still a great challenge to develop CPL materials with color tunability using chiral molecules due to tedious synthesis. Recently, Jiang reported a single molecular system **27** (Chol–CN–Py) consisting of a pyridine-functionalized cyanostilbene unit, a chiral cholesterol moiety and an ester linker.[76] Chol–CN–Py could gelatinize in DMSO by virtue of the synergistic effects of van der Waals forces and π–π interactions between cholesterol and the cyanostilbene group. The structure of the gel was further investigated by SEM and the result showed that the twisted configuration of the left-handed nanohelix fibers provided a tangled 3D network, suggesting an ordered chiral expression in the microstructure. Based on the results obtained from X-ray diffraction and the calculated *d*-spacing values from Bragg's law, compound **27** formed a bilayer self-assembly structure driven by π–π stacking interaction, which served as the basic unit of the nanofibers. As a result, the chiral supramolecular gel emitted intense blue CPL and exhibited a large g_{em} value of -3.0×10^{-2}. Upon exposure to different amounts of trifluoroacetic acid, the emission of the xerogel film of **27** was tuned from blue to yellow owing to the protonation of the pyridine unit. In addition, the blue emission could be recovered upon fuming with triethylamine vapor due to deprotonation. Such a reversible process could be repeated many times.

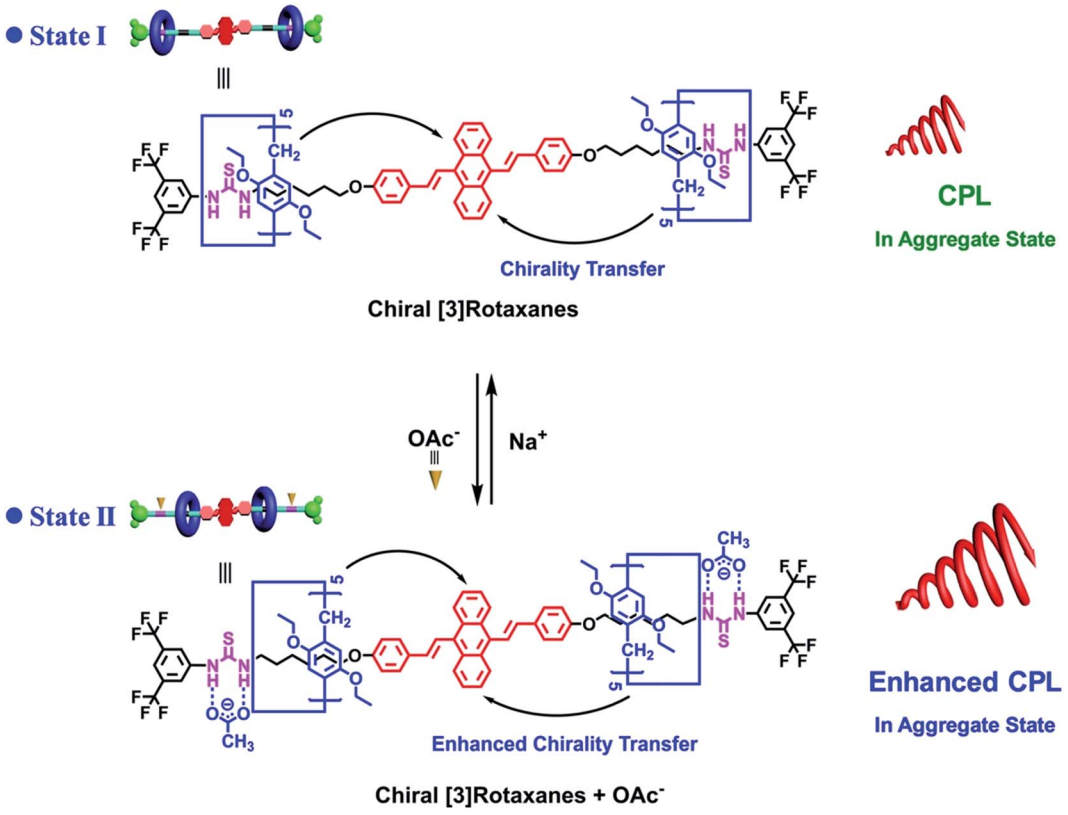

Fig. 14 Mechanism for the switchable circularly polarized luminescence (CPL) system based on the AIE-active chiral [3]rotaxanes **26**. Reprinted from ref. 75 with permission. Copyright 2021 Wiley-VCH.

Most of the CD spectra are obtained in solution but such measurements may not be suitable for TPE derivatives without chiral pendants due to their fast reversible configurational change. TPE is a propeller-like molecule with four phenyl rings rotating in one direction (clockwise or anticlockwise). The *P*- or *M*-helical chirality of the TPE-based atropisomers stems from the mirror symmetry breaking (MSB), and their CD and CPL spectra can be characterized by solid-state chiroptical techniques. For example, Zhang mixed three TPE derivatives (TPE **29**, BETPE **30** and TETPE **31**) with KBr pellets to analyze their solid-state CD spectra and discriminate the *P*- or *M*-helicity of TPE.[40] These compounds showed no chirality in solution due to the fast rotations of the phenyl rings. However, in the solid state, the raceme can be separated by MSB to give TPE showing *P*- or *M*-helicity (Fig. 15A and B). The CD spectra were recorded by doping different mass concentrations (1/1000, 1/800, and 1/400) of *M*-TPE, *P*-BETPE and *M*-BETPE with KBr pellets, respectively (Fig. 15C–E), and it was found that the CD intensity could reach the maximum at an appropriate concentration.

The immobilization of TPE propeller-like conformation can not only provide a couple of enantiomers by raceme separation but also strengthen the fluorescence efficiency in solution to provide the direct evidence for the AIE mechanism. Taking this into account, Zheng synthesized a TPE-based tetracycle **32** by covalent bond connection.[79] As expected, the racemic tetracycle **32** could be separated into a set of enantiomers by chiral HPLC. As shown in Fig. 16A, one crystal structure was left-handed (*M*-**32**), and the other displayed right-handed helicity (*P*-**32**). According to the restriction of molecular rotation (RIR) as the mechanism of the AIE effect, **32** fluoresced strongly in THF solution with a PLQY of 97% (Fig. 16B). While the CD spectrum of *M*-**32** showed an intense positive Cotton effect, that of *P*-**32** exhibited a mirror image with a similar intensity (Fig. 16C). Moreover, obvious CPL signals of *M*-**32** and *P*-**32** with mirror images were detected in THF solution and suspension at about 505 nm (Fig. 16D). The calculated g_{em} values of *M*-**32** and *P*-**32** were $+3.1 \times 10^{-3}$ and -3.3×10^{-3}, respectively. Such high PLQY and dissymmetry factors endow *M*-**32** and *P*-**32** with potential to be applied in 3D displays and medical imaging. To enhance the g_{em} value of monomeric molecules, a general approach is to self-assemble the fluorophores into supramolecular nanostructures such as helical nanofibers.[96,97] Recently, another new TPE-based tetracycle tetramine **33** was reported by Zheng, which could be resolved into two enantiomers *M*-**33** and *P*-**33** with a single helical direction.[80] When 4-dodecylbenzenesulfonic acid (DSA) was added to a 1,2-dichloroethane solution and film of **33**, the resulting *M*-**33**-DSA and *P*-**33**-DSA were found to show significantly enhanced CPL and g_{em} values. *M*-**33**-DSA formed

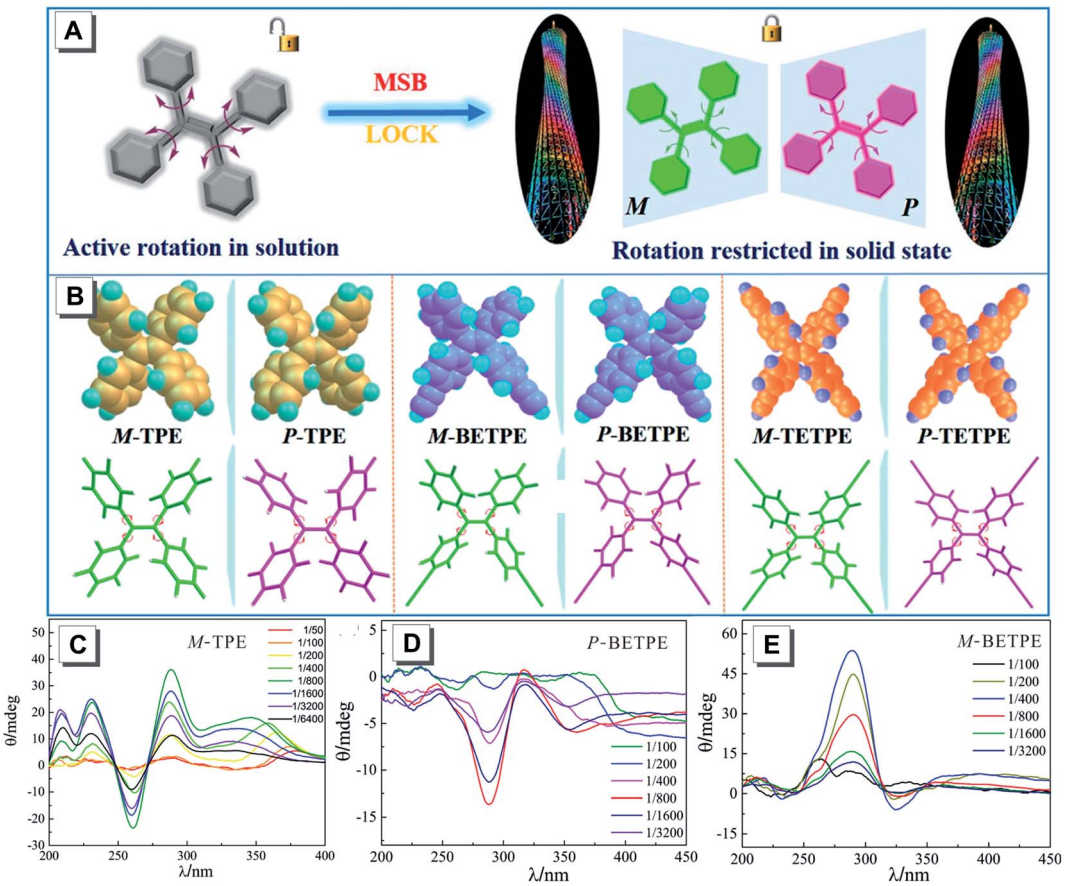

Fig. 15 (A) Immobilization of the free rotation of TPE in the solid state can generate helical chirality. (B) The optimized conformations of TPE, BETPE, and TETPE. Solid-state CD spectra of (C) TPE, (D) *P*-BETPE, and (E) *M*-BETPE at various weight ratios. Adapted from ref. 40 with permission. Copyright 2017 American Chemical Society.

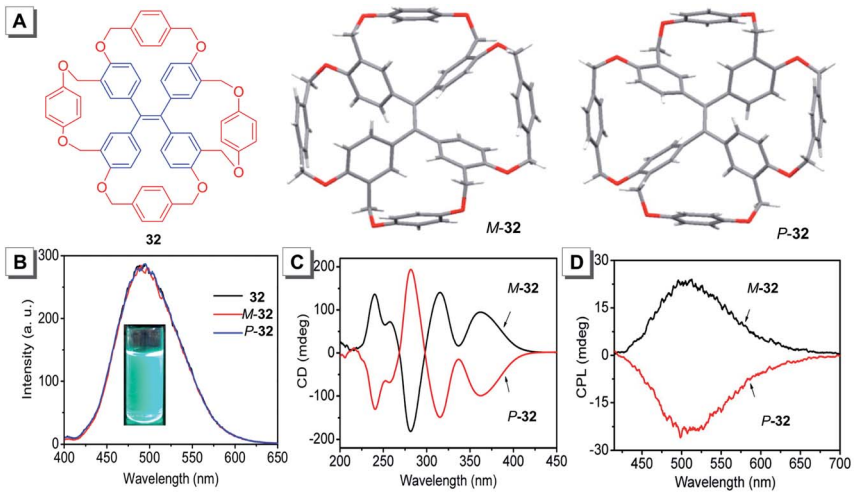

Fig. 16 (A) Molecular structure of **32** and its crystal structures. (B) PL spectra of racemic-**32**, *M*-**32** and *P*-**32** in THF ([**32**] = 5.0×10^{-5} M). (C) CD spectra and (D) CPL spectra of *M*-**32** and *P*-**32** in THF ([**32**] = 1.0×10^{-3} M). Adapted from ref. 79 with permission. Copyright 2016 American Chemical Society.

microribbons owing to noncovalent interactions such as hydrogen bonds, ArH-π interactions, van der Waals forces, *etc.*, between molecules. Simultaneously, the ribbons could coil into a right-handed helical nanofiber driven by the propeller-like conformation of the immobilized TPE units. The further self-assembly with one enantiomer of tartaric acid generated over 200-fold CPL enhancement with a very high g_{em} value of up to 0.61.

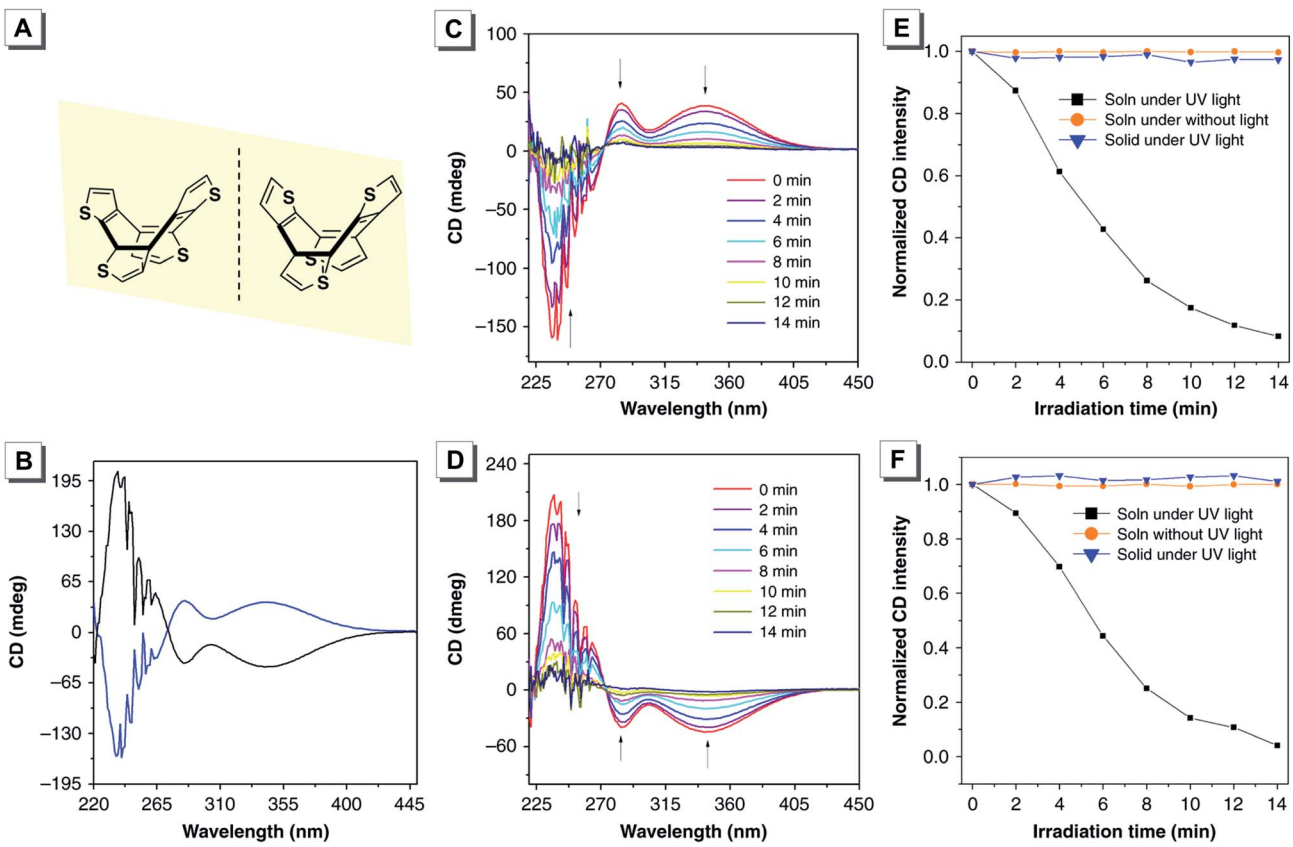

Fig. 17 (A) Molecular structures and (B) CD spectra of the two enantiomers of **37** in THF solution. (C and D) The changes of CD spectra of the two enantiomers in THF solution under UV irradiation for different times. (E and F) Time-dependent CD spectral change profiles of the two enantiomers in THF solution and the solid state with or without UV irradiation. Adapted from ref. 42 with permission. Copyright 2019 Nature Publishing Group.

The RIR principle can explain the AIE effect of most molecular systems but is not applicable for some luminogens without rotors. After an in-depth investigation and study, the restriction of intramolecular vibrations (RIV) has been proposed for the AIE phenomenon of many rotor-free AIEgens.[98,99] A non-aromatic annulene derivative of cyclooctatetrathiophene **37** was reported by Tang, and was a new vibrational AIE system without any rotors.[42] The CD spectra of the two enantiomers of **37** in THF solution showed strong absorption peaks with good mirror symmetry (Fig. 17B). The CD signals gradually decreased and completely racemized when UV irradiated for 14 min, suggesting that the two enantiomers were racemizable in the solution state upon light irradiation (Fig. 17C and D). In contrast, their CD spectra remained unchanged in the solid state even in the presence of UV irradiation, indicating that the up–down conformational inversion could be suppressed in the solid state (Fig. 17E and F). In addition, obvious CPL signals of the enantiomers were recorded in the crystalline state with a g_{em} value of about 10^{-3}.

Luminescent materials with a controllable emission color and CPL are hardly accessible for achiral AIEgens alone. In 2019, Tang developed a novel strategy for the construction of white emission and tunable CPL by the interactions of achiral AIEgens and host polymers.[44] Upon slow evaporation of a solution of helical polymer **44** and achiral AIEgen **33**, the polymer chains of **44** transformed into crystalline lamellae and meanwhile blue-emissive crystalline and yellow-emissive amorphous nano-aggregates of **43** were formed (Fig. 18A and B). As shown in Fig. 18C, the bands in the spiral spherulites reflected the radial growth of the twisted lamellae due to the imbalanced stress at the opposite folding surface. As a result, white CPL emission was ultimately generated. The chiroptical properties of the spiral polymer film were further investigated by CPL spectroscopy. A negative CPL with a g_{em} value of -2×10^{-3} was produced from the ACW spherulites, while a positive CPL signal was obtained from the CW ones *via* film inversion.

Some achiral AIEgens were incorporated into LCs to explore their CPL. For example, Tang reported chiral nematic liquid crystals (N*LC) showing excellent CPL performance by doping 0.5 wt% of achiral AIEgen **47** into LCs.[87] The reflection spectra revealed that the planar aligned N*LC and PL-N*LC cells with 0.5 wt% of 47 exhibited little change of the stop band (Fig. 19B). CD spectra were coincident with the reflection spectra and showed different absorption in the corresponding region (Fig. 19C). These results demonstrated that the N*-LC and PL-N*-LC cells possessed the same helical chirality and the observed colors in both cases originated from the selective reflection of the CPL. This N*LC with 0.5 wt% of **47** was suitable to fabricate a CPL-active liquid crystalline display (LCD). A maximum dissymmetry factor g_{em} of 0.4 was obtained in such LCD under no electric field conditions (Fig. 19D).

4.2 CPOLED

The development of CPOLEDs has attracted much attention due to their excellent emission efficiency and high contrast in 3D displays.[66,68,69] Ye designed binaphthyl derivatives *R*/*S*-**15** that

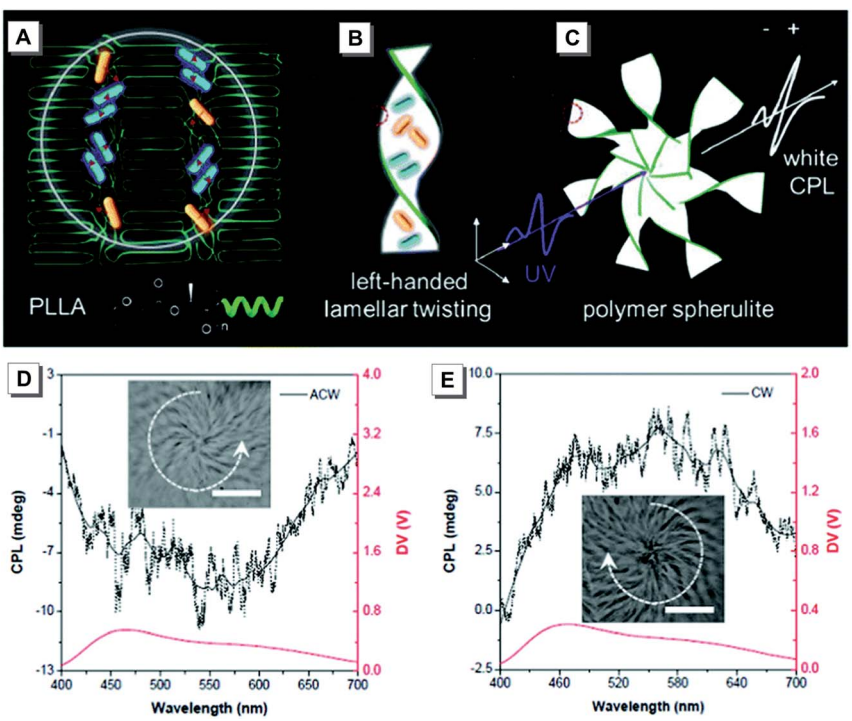

Fig. 18 (A) White emission from **43** packed in the amorphous region between polymer crystalline lamellae. (B and C) The formation of 3D spiral banded spherulites and the generation of CPL. (D and E) The CPL spectrum switching by the inversion of the P-PLLA film. Insets: Bright-field images of 3D spiral patterns of the spherulites from two different sides. Adapted from ref. 44 with permission. Copyright 2019 the Royal Society of Chemistry.

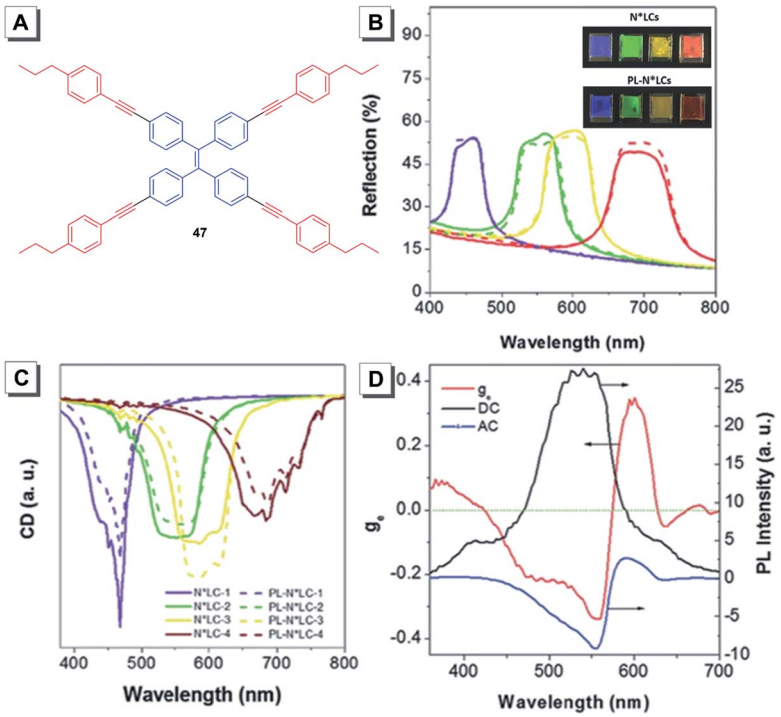

Fig. 19 (A) Molecular structure of **47**. (B) Reflection spectra of the nematic liquid crystals (N*LCs) (solid lines) and PL-N*LC (dashed lines) cells with right-handed CPL. In the PL-N*LC cells, the concentration of **47** in the N*LC host was 0.5 wt%. Inset: Photographs of PL-N*LC cells and N*LC cells taken under natural light. (C) CD spectra of the PL-N*LC (dashed lines) and N*LC (solid lines). (D) CPL dissymmetry factor g_{em}, AC, and DC curves of the PL-N*LC cells prepared from N*LC-3 and **47** with a weight ratio of 0.5 wt%. AC $= I_L - I_R$, DC $= (I_L + I_R)/2$, and g_{em} = AC/DC. Ratio of N*LC-3: SCL1717/CB15 = 0.64/0.36. Adapted from ref. 87 with permission. Copyright 2016 Wiley-VCH.

were non-emissive in THF solution but their aggregates formed in water emitted bright yellow fluorescence with a high quantum yield of 32.1%.[66] The CD spectra of *R*/*S*-**15** were investigated in THF solution, aggregates and spin-coated films, which showed good mirror-imaged CD bands in their corresponding UV absorption regions. Their CPL was also studied while no CPL signal was detected in THF, and obvious mirror-imaged CPL bands were observed in their spin-coated films with a g_{em} value of 2.8×10^{-3}. This demonstrated a typical AICPL characteristic. Doping-free CPOLEDs were fabricated by using *R*/*S*-**15** as an emitter. The devices exhibited a low turn-on voltage of 3.18 V, a high maximum brightness of 8061 cd m^{-2} and a low EQE of 0.48%. The calculated dissymmetry factors of the CPOLEDs were $+3.2 \times 10^{-3}$ and -3.0×10^{-3} for devices *S*-**15** and *R*-**15**, respectively.

Tang utilized a series of chiral AIEgens **17–20** with binaphthyl moieties and carbazole units to prepare a set of highly efficient CPOLEDs with delayed fluorescence (Fig. 20A).[68] The single crystal structures of *R*-**17**, *S*-**19**, and *S*-**20** revealed that these chiral molecules adopt twisted conformations which resulted in their AIE properties (Fig. 20B). As illustrated in Fig. 20C, these AIEgens showed AIE and twisted intramolecular charge transfer effects in THF/H_2O mixtures. Moreover, these AIEgens emitted bright yellow fluorescence in the solid powder. Their chiroptical properties were investigated by using CD and CPL (Fig. 20D and E). Mirror images of the Cotton effect and CPL spectra were detected. The CPOLEDs prepared by utilizing the neat and doped films of the molecules showed quite high external quantum yields (EQE) of 3.5% and 9.3%, respectively. The devices based on doped films of *S*-**17**, *S*-**18**, *S*-**19** and *S*-**20** emitted strong yellowish-green electroluminescence. The current–voltage–luminance characteristics of the CPOLEDs exhibited low turn-on voltages and a high luminance of up to 2948 cd m^{-2}. In addition, the calculated dissymmetry factors g_{EL} of these devices were +0.025, +0.027, and +0.016 for *S*-**18**, *S*-**19** and *S*-**20** and −0.030, −0.027, and −0.027 for *R*-**18**, *R*-**19** and *R*-**20**, respectively.

Up to now, most research work on CPOLEDs has focused on bottom-emission devices.[100] However, it is quite difficult to fabricate high-resolution displays by bottom-emission CPOLED technology using the silicon wafer processing method. In contrast, top-emission OLEDs are more feasible for practical applications. Recently, Pieters reported the first top-emission CPOLEDs by utilizing compound **21** as an emitter.[69] To maximize the chiral perturbation efficiency, compound **21** was designed by placing the carbazole unit near the binaphthyl unit, and study on its photophysical properties showed that it exhibited typical thermally activated delayed fluorescence. Fig. 21a demonstrates a typical CPOLED stacked with *S*-**21** and *R*-**21** as chiral emitters, which emitted bright green emission at 510 nm (Fig. 21b and c). The CPOLED manifested a low leakage current (≤1 μA cm^{-2}) and a high brightness of 6000 cd m^{-2} at 11 V, and the corresponding current efficiency could reach up to 2.5 cd A^{-1} with an EQE of 0.8% (Fig. 21d). Overall, the top-

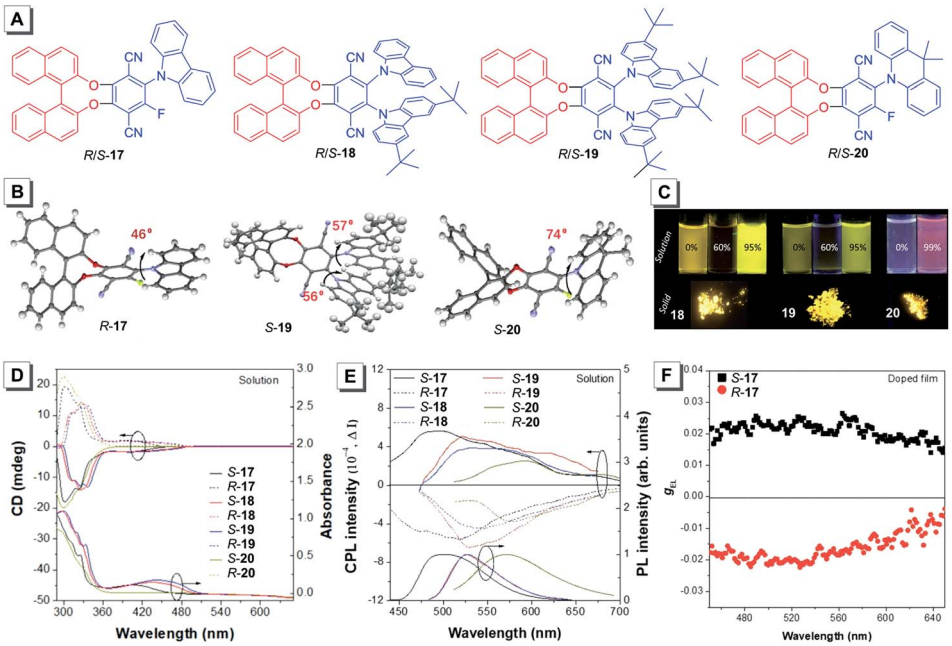

Fig. 20 (A) Molecular structures of **17**–**20**. (B) Crystal structures of *R*-**17**, *S*-**19**, and *S*-**20**. (C) Fluorescence photos of *S*-**18**, *S*-**19**, and *S*-**20** in THF and H_2O mixtures with different water fractions and in solid powder under a UV lamp. (D) CD and (E) CPL spectra of *R*/*S*-**17**–**20** in toluene. (F) Dissymmetry factors g_{EL} of *R*/*S*-**17** in neat films. Adapted from ref. 68 with permission. Copyright 2018 Wiley-VCH.

emission CPOLEDs showed great promise for manufacturing high-resolution displays based on silicon wafer processing and many other photonic applications.

4.3 Chiral recognition

Chiral AIEgens can enantioselectively complex with enantiomers to generate diastereomers with differential fluorescence

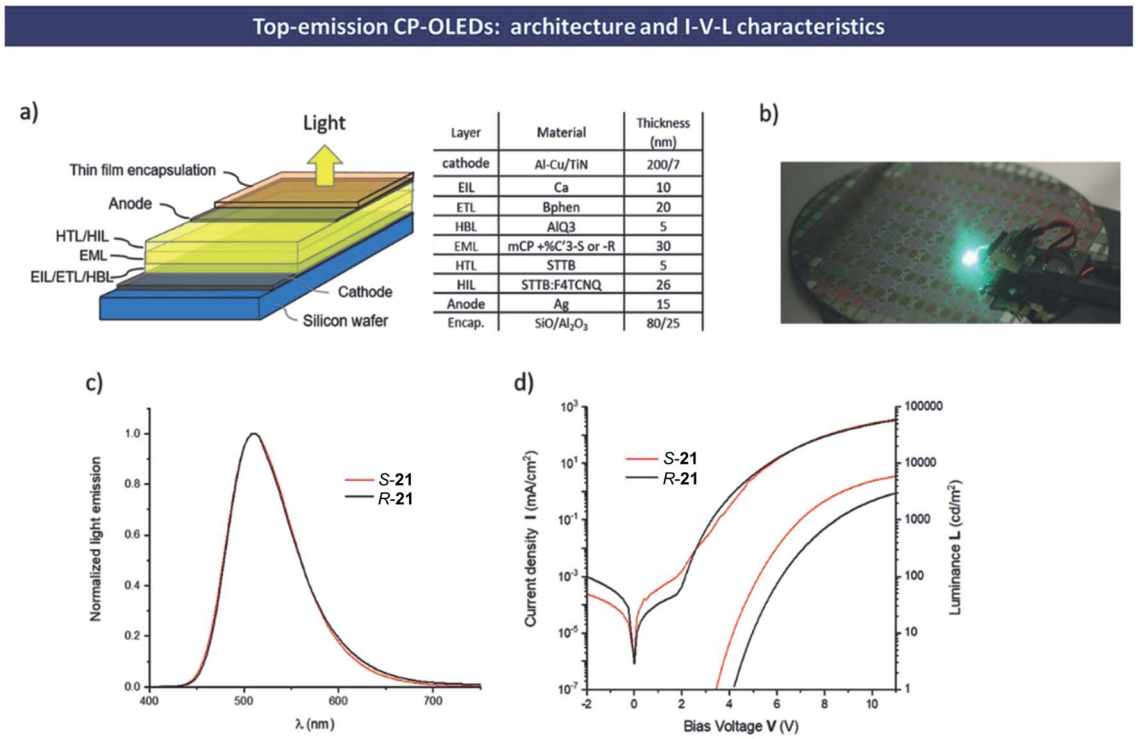

Fig. 21 (a) Device structure of a top-emission CP-OLED built from a typical thin film stacked with *R*-**21** and *S*-**21** chiral dopants. (b) The test of an individual CPOLED in 8 inch wafer level-processed CP-OLEDs. (c) Light emission spectrum of CP-OLEDs integrating either *S*-**21** or *R*-**21** chiral dopants; (d) corresponding *I*–*V*–*L* characteristics. Adapted from ref. 69 with permission. Copyright 2020 Wiley-VCH.

intensities through supramolecular interactions, such as hydrogen bonding, coordinative bonding, hydrophobic interactions and electrostatic interactions. Thus, the signal change can be recorded by using a fluorescence spectrometer. A good chiral sensor should meet the requirements of high sensitivity and selectivity. In the past few decades, many chiral fluorescent sensors were reported. Nevertheless, most of them suffered from either low sensitivity or the ACQ effect, which impeded their further application. Since the discovery of the AIE phenomenon, many efforts have been made to design new chiral AIE-active sensors. Up to now, a lot of fluorescent probes with AIE characteristics have been successfully developed. For example, Zheng prepared chiral AIEgens for chiral recognition.[77,78] The chiral compounds D/L-**28A** bearing tartaric acid groups were synthesized in excellent yields without the use of column chromatography. D/L-**28A** exhibited strong fluorescence only in aggregates, which allowed them to discriminate different enantiomers *via* fluorescence change. According to acid–base interaction, a series of chiral amines were studied. As shown in Fig. 22, L-**28A** could form aggregates with (1*R*,2*S*)-**56** in an appropriate solvent and emitted intense blue fluorescence. However, when an equal volume of L-**28A** was mixed with (1*S*,2*R*)-**56**, the solution remained clear and was non-fluorescence even after standing for more than 1 day. In an ethanol/water mixture (1 : 9, v/v), both enantiomers of chiral amine (1*R*,2*S*)-**56** and (1*S*,2*R*)-**56** could self-assemble with D-**28A** to display different aggregation morphologies. SEM revealed

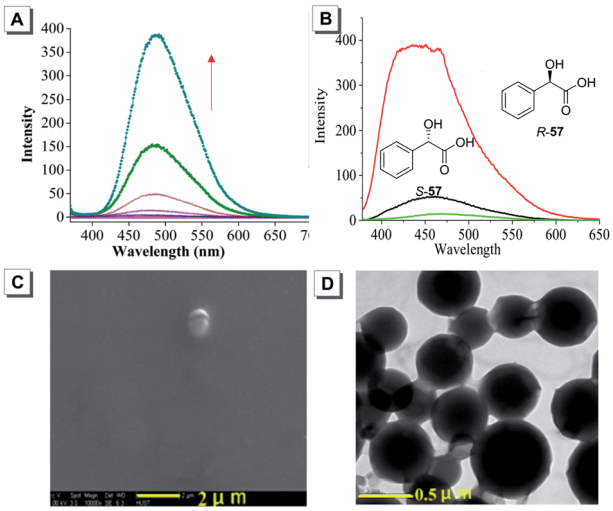

Fig. 23 (A) PL spectra of (1*S*,2*S*)-**7** in a mixture of THF and water with increasing water fraction. (B) PL spectra of (1*S*,2*S*)-**7** interacting with mandelic acid **57**. (C) SEM image of (1*S*,2*S*)-**7** with *S*-**57**. (D) TEM image of (1*S*,2*S*)-**7** with *R*-**57**. Adapted from ref. 54 with permission. Copyright 2015 American Chemical Society.

that aggregates were formed from D-**28A** and (1*S*,2*R*)-**56** consisting nanofibers with a length of about 50 μm and a width of about 200 nm (Fig. 22C). Nevertheless, the aggregates made from D-**28A** and (1*R*,2*S*)-**56** were composed of round nanospheres with a diameter of 100–500 nm (Fig. 22D).

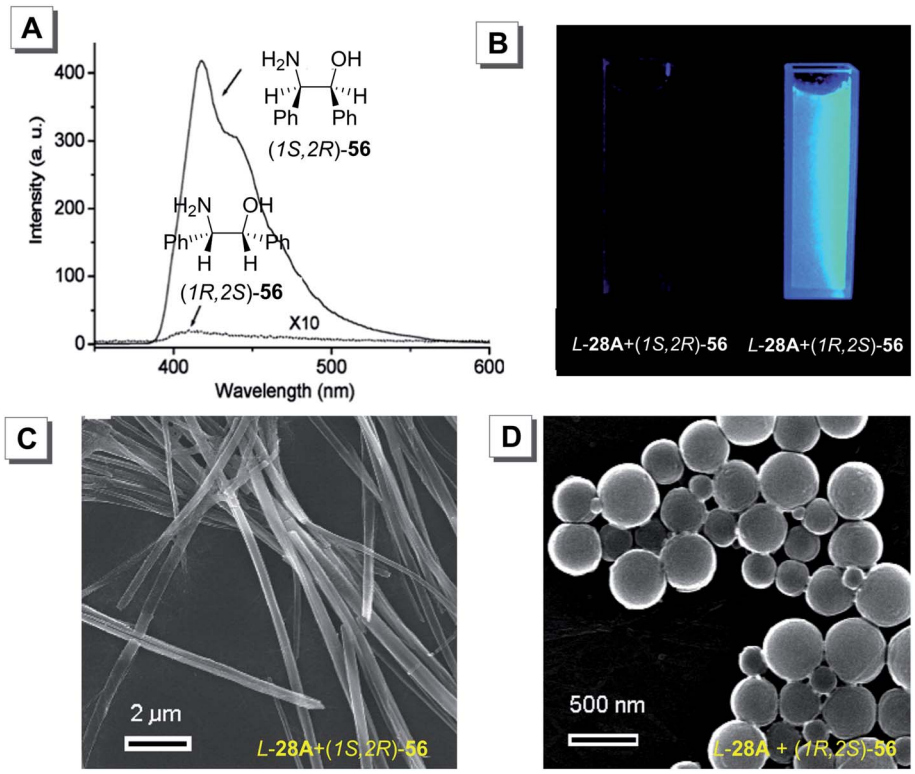

Fig. 22 (A) PL spectra of L-**28A** interacting with enantiomers of **56**. (B) Fluorescence images of L-**28A** interacting with enantiomers of **56**. SEM images of (C) L-**28A** + (1*S*,2*R*)-**56** and (D) L-**28A** + (1*R*,2*S*)-**56**, respectively. Adapted from ref. 77 with permission. Copyright 2011 American Chemical Society.

To widen the applicability of chiral AIE receptors to more chiral analytes, TPE macrocycle **7** displaying the AIE effect was synthesized by tethering an optically pure diphenyldiaminoethylene group.[54] The additional cavity of the macrocycle is anticipated to enhance the selectivity for analytes. Indeed, the AIE macrocycle **7** could discriminate a series of chiral acids and α-amino acids by enantioselective aggregation. As disclosed by SEM and TEM, there existed different aggregation states between mixtures of (1*S*,2*S*)-**7** and the two enantiomers of mandelic acid **57**. The mixture of (1*S*,2*S*)-**7** and *S*-**57** displayed almost no uniform nanostructures (Fig. 23C), while that of (1*S*,2*S*)-**7** and *R*-**57** formed nanospheres with an average diameter of 400 nm (Fig. 23D).

5. Conclusions and outlook

Since its discovery in 2001, AIE has fused into many conventional research fields, such as optoelectronic devices, chemo/biosensors and so on. As a relatively new research field, chiral materials with AIE characteristics have attracted increasing interest. In this review, we mainly discussed chiral materials with aggregation-induced emission including their molecular structures, self-assembly and functions. Generally, chiral AIEgens were composed of AIE-active backbones and chiral units. Moreover, latent chiral AIEgens with molecular rotors or vibrators could exhibit chirality upon breaking the mirror symmetry. The chirality of many achiral AIEgens can also be induced by some optically active molecules through non-covalent interactions. From the molecular level to supramolecular systems, chiral AIEgens could assemble into helical architectures accompanied by enhanced g_{em} values. Meanwhile, the phenomena of aggregation-induced CD and CPL were often observed during the self-assembly process. CD and CPL spectroscopies are useful techniques to investigate the chiral molecule in the ground state and excited state, respectively. On the basis of CPL, the development of highly efficient CPOLEDs is attracting more and more attention due to their practical applications in 3D displays. On the other hand, chiral recognition can enable rapid enantioselective determination of amines, amino alcohols, amino acids, α-hydroxycarboxylic acids and so on. By utilizing the AIE effect, many chiral "turn-on" sensors were successfully developed in the past decade. In the future, it is anticipated that more chiral AIEgens with novel structures and properties will be designed and synthesized. Although many excellent studies on CPL have been reported, we still need to decipher the structure–property relationship clearly and develop an effective strategy to design chiral AIEgens with high emission efficiency and high dissymmetry factors. Research on CPOLEDs based on chiral AIEgens is still at the initial stage. Thus, much attention should be paid to highly efficient CPOLEDs with large dissymmetry factors and high external quantum yields. Moreover, it is still a great challenge to develop AIE-active chiral sensors with high enantioselectivity and enantiosensitivity in the future.

Author contributions

CL and JCY contributed equally to this work. All of the authors participated in this review work. BZT, HTF and CL proposed and designed the review. CL and JCY prepared the draft. JWYL and HTF finally revised the review.

Conflicts of interest

The authors declare no competing financial interests.

Acknowledgements

This work was partially supported by the National Natural Science Foundation of China (21788102 and 21805002), the Research Grants Council of Hong Kong (N-HKUST609/19, 16305518, 16307020, C6009-17G and C6014-20W), the Innovation and Technology Commission (ITC-CNERC14SC01), the Natural Science Foundation of Guangdong Province (2019B121205002), and the Guangdong Basic and Applied Basic Research Foundation (2020A1515110476).

References

1 W. Xiao, K. H. Ernst, K. Palotas, Y. Zhang, E. Bruyer, L. Peng, T. Greber, W. A. Hofer, L. T. Scott and R. Fasel, *Nat. Chem.*, 2016, **8**, 326–330.
2 Q. Gan, X. Wang, B. Kauffmann, F. Rosu, Y. Ferrand and I. Huc, *Nat. Nanotechnol.*, 2017, **12**, 447–452.
3 J. Ren, Y. Hu, C. H. Lu, W. Guo, M. A. A. Garcia, F. Ricci and I. Willner, *Chem. Sci.*, 2015, **6**, 4190–4195.
4 M. B. Avinash and T. Govindaraju, *Nanoscale*, 2014, **6**, 13348–13369.
5 L. A. Nguyen, H. He and C. Pham-Huy, *Int. J. Biomed. Sci.*, 2006, **2**, 85–100.
6 T. Ito and H. Handa, *Congenital Anomalies*, 2012, **52**, 1–7.
7 W. Liu, J. Gan, D. Schlenk and W. A. Jury, *Proc. Natl. Acad. Sci. U. S. A.*, 2005, **102**, 701–706.
8 A. Accetta, R. Corradini and R. Marchelli, *Top. Curr. Chem.*, 2011, **300**, 175–216.
9 F. Pop, N. Zigon and N. Avarvari, *Chem. Rev.*, 2019, **119**, 8435–8478.
10 X. Mei and C. Wolf, *J. Am. Chem. Soc.*, 2004, **126**, 14736–14737.
11 H. M. Seifert, Y. B. Jiang and E. V. Anslyn, *Chem. Commun.*, 2014, **50**, 15330–15332.
12 H. H. Jo, C. Y. Lin and E. V. Anslyn, *Acc. Chem. Res.*, 2014, **47**, 2212–2221.
13 J. Heo and C. A. Mirkin, *Angew. Chem., Int. Ed.*, 2006, **45**, 941–944.
14 M. Caricato, N. J. Leza, K. Roy, D. Dondi, G. Gattuso, L. S. Shimizu, D. A. Vander Griend and D. Pasini, *Eur. J. Org. Chem.*, 2013, 6078–6083.
15 K. W. Bentley and C. Wolf, *J. Am. Chem. Soc.*, 2013, **135**, 12200–12203.
16 M. Agnes, A. Nitti, D. A. Vander Griend, D. Dondi, D. Merli and D. Pasini, *Chem. Commun.*, 2016, **52**, 11492–11495.

17 D. Pasini and A. Nitti, *Chirality*, 2016, **28**, 116–123.
18 M. Anyika, H. Gholami, K. D. Ashtekar, R. Acho and B. Borhan, *J. Am. Chem. Soc.*, 2014, **136**, 550–553.
19 L. Pu, *Chem. Rev.*, 2004, **104**, 1687–1716.
20 X. Zhang, J. Yin and J. Yoon, *Chem. Rev.*, 2014, **114**, 4918–4959.
21 S. Yu and L. Pu, *Tetrahedron*, 2015, **71**, 745–772.
22 L. Pu, *Acc. Chem. Res.*, 2012, **45**, 150–163.
23 J. Roose, B. Z. Tang and K. S. Wong, *Small*, 2016, **12**, 6495–6512.
24 N. Berova, L. Di Bari and G. Pescitelli, *Chem. Soc. Rev.*, 2007, **36**, 914–931.
25 S. M. Kelly and N. C. Price, *Curr. Protein Pept. Sci.*, 2000, **1**, 349–384.
26 J. P. Riehl and F. S. Richardson, *Chem. Rev.*, 1986, **86**, 1–16.
27 J. Weiss, *Nature*, 1943, **152**, 176–178.
28 J. Luo, Z. Xie, J. W. Lam, L. Cheng, H. Chen, C. Qiu, H. S. Kwok, X. Zhan, Y. Liu, D. Zhu and B. Z. Tang, *Chem. Commun.*, 2001, 1740–1741.
29 S. Song, H.-F. Zheng, H.-T. Feng and Y.-S. Zheng, *Chem. Commun.*, 2014, **50**, 15212–15215.
30 H.-T. Feng, J.-B. Xiong, J. Luo, W.-F. Feng, D. Yang and Y.-S. Zheng, *Chem.–Eur. J.*, 2017, **23**, 644–651.
31 X. Feng, C. Qi, H.-T. Feng, Z. Zhao, H. H. Y. Sung, I. D. Williams, R. T. K. Kwok, J. W. Y. Lam, A. Qin and B. Z. Tang, *Chem. Sci.*, 2018, **9**, 5679–5687.
32 H.-T. Feng, J.-H. Wang and Y.-S. Zheng, *ACS Appl. Mater. Interfaces*, 2014, **6**, 20067–20074.
33 G. Niu, R. Zhang, J. P. C. Kwong, J. W. Y. Lam, C. Chen, J. Wang, Y. Chen, X. Feng, R. T. K. Kwok, H. H. Y. Sung, I. D. Williams, M. R. J. Elsegood, J. Qu, C. Ma, K. S. Wong, X. Yu and B. Z. Tang, *Chem. Mater.*, 2018, **30**, 4778–4787.
34 R. T. Kwok, C. W. Leung, J. W. Lam and B. Z. Tang, *Chem. Soc. Rev.*, 2015, **44**, 4228–4238.
35 Y. Hong, J. W. Y. Lam and B. Z. Tang, *Chem. Soc. Rev.*, 2011, **40**, 5361–5388.
36 J. Mei, Y. Hong, J. W. Y. Lam, A. Qin, Y. Tang and B. Z. Tang, *Adv. Mater.*, 2014, **26**, 5429–5479.
37 H.-T. Feng, Y.-X. Yuan, J.-B. Xiong, Y.-S. Zheng and B. Z. Tang, *Chem. Soc. Rev.*, 2018, **47**, 7452–7476.
38 J.-B. Xiong, Y.-X. Yuan, L. Wang, J.-P. Sun, W.-G. Qiao, H.-C. Zhang, M. Duan, H. Han, S. Zhang and Y.-S. Zheng, *Org. Lett.*, 2018, **20**, 373–376.
39 H.-T. Feng, C. Liu, Q. Li, H. Zhang, J. W. Y. Lam and B. Z. Tang, *ACS Mater. Lett.*, 2019, **1**, 192–202.
40 D. Li, R. Hu, D. Guo, Q. Zang, J. Li, Y. Wang, Y.-S. Zheng, B. Z. Tang and H. Zhang, *J. Phys. Chem. C*, 2017, **121**, 20947–20954.
41 S. Xue, L. Meng, R. Wen, L. Shi, J. W. Lam, Z. Tang, B. S. Li and B. Z. Tang, *RSC Adv.*, 2017, **7**, 24841–24847.
42 Z. Zhao, X. Zheng, L. Du, Y. Xiong, W. He, X. Gao, C. Li, Y. Liu, B. Xu, J. Zhang, F. Song, Y. Yu, X. Zhao, Y. Cai, X. He, R. T. K. Kwok, J. W. Y. Lam, X. Huang, D. Lee Phillips, H. Wang and B. Z. Tang, *Nat. Commun.*, 2019, **10**, 2952.
43 M. Khorloo, Y. Cheng, H. Zhang, M. Chen, H. H. Y. Sung, I. D. Williams, J. W. Y. Lam and B. Z. Tang, *Chem. Sci.*, 2020, **11**, 997–1005.
44 Y. Cheng, S. Liu, F. Song, M. Khorloo, H. Zhang, R. T. K. Kwok, J. W. Y. Lam, Z. He and B. Z. Tang, *Mater. Horiz.*, 2019, **6**, 405–411.
45 J. Han, J. You, X. Li, P. Duan and M. Liu, *Adv. Mater.*, 2017, **29**, 1606503.
46 D. N. Nadimetla, M. Al Kobaisi, S. T. Bugde and S. V. Bhosale, *Chem. Rec.*, 2020, **20**, 793–819.
47 Z. Zhao, B. He and B. Z. Tang, *Chem. Sci.*, 2015, **6**, 5347–5365.
48 J. Liu, H. Su, L. Meng, Y. Zhao, C. Deng, J. C. Y. Ng, P. Lu, M. Faisal, J. W. Y. Lam, X. Huang, H. Wu, K. S. Wong and B. Z. Tang, *Chem. Sci.*, 2012, **3**, 2737–2747.
49 J. C. Y. Ng, H. Li, Q. Yuan, J. Liu, C. Liu, X. Fan, B. S. Li and B. Z. Tang, *J. Mater. Chem. C*, 2014, **2**, 4615–4621.
50 H. Li, S. Xue, H. Su, B. Shen, Z. Cheng, J. W. Lam, K. S. Wong, H. Wu, B. S. Li and B. Z. Tang, *Small*, 2016, **12**, 6593–6601.
51 J. C. Y. Ng, J. Liu, H. Su, Y. Hong, H. Li, J. W. Y. Lam, K. S. Wong and B. Z. Tang, *J. Mater. Chem. C*, 2014, **2**, 78–83.
52 H. Li, J. Cheng, H. Deng, E. Zhao, B. Shen, J. W. Y. Lam, K. S. Wong, H. Wu, B. S. Li and B. Z. Tang, *J. Mater. Chem. C*, 2015, **3**, 2399–2404.
53 N. N. Liu, S. Song, D. M. Li and Y. S. Zheng, *Chem. Commun.*, 2012, **48**, 4908–4910.
54 H.-T. Feng, X. Zhang and Y.-S. Zheng, *J. Org. Chem.*, 2015, **80**, 8096–8101.
55 H.-T. Feng and Y.-S. Zheng, *Chem.–Eur. J.*, 2014, **20**, 195–201.
56 H.-T. Feng, S. Song, Y.-C. Chen, C.-H. Shen and Y.-S. Zheng, *J. Mater. Chem. C*, 2014, **2**, 2353–2359.
57 S. P. Goskulwad, M. A. Kobaisi, D. D. La, R. S. Bhosale, M. Ratanlal, S. V. Bhosale and S. V. Bhosale, *Chem.–Asian J.*, 2018, **13**, 3947–3953.
58 Q. Xia, L. Meng, T. He, G. Huang, B. S. Li and B. Z. Tang, *ACS Nano*, 2021, **15**, 4956–4966.
59 Q. Ye, D. Zhu, H. Zhang, X. Lu and Q. Lu, *J. Mater. Chem. C*, 2015, **3**, 6997–7003.
60 L. Pu, *Tetrahedron: Asymmetry*, 1998, **9**, 1457–1477.
61 X. Liu, J. Jiao, X. Jiang, J. Li, Y. Cheng and C. Zhu, *J. Mater. Chem. C*, 2013, **1**, 4713–4719.
62 C. Zhang, M. Li, H.-Y. Lu and C.-F. Chen, *RSC Adv.*, 2018, **8**, 1014–1021.
63 H.-T. Feng, X. Gu, J. W. Y. Lam, Y.-S. Zheng and B. Z. Tang, *J. Mater. Chem. C*, 2018, **6**, 8934–8940.
64 S. Zhang, Y. Wang, F. Meng, C. Dai, Y. Cheng and C. Zhu, *Chem. Commun.*, 2015, **51**, 9014–9017.
65 H. Zhang, H. Li, J. Wang, J. Sun, A. Qin and B. Z. Tang, *J. Mater. Chem. C*, 2015, **3**, 5162–5166.
66 X. Zhang, Y. Zhang, H. Zhang, Y. Quan, Y. Li, Y. Cheng and S. Ye, *Org. Lett.*, 2019, **21**, 439–443.
67 J. Zhang, Q. Liu, W. Wu, J. Peng, H. Zhang, F. Song, B. He, X. Wang, H. H. Sung, M. Chen, B. S. Li, S. H. Liu, J. W. Y. Lam and B. Z. Tang, *ACS Nano*, 2019, **13**, 3618–3628.

68 F. Song, Z. Xu, Q. Zhang, Z. Zhao, H. Zhang, W. Zhao, Z. Qiu, C. Qi, H. Zhang, H. H. Y. Sung, I. D. Williams, J. W. Y. Lam, Z. Zhao, A. Qin, D. Ma and B. Z. Tang, *Adv. Funct. Mater.*, 2018, **28**, 1800051.
69 L. Frédéric, A. Desmarchelier, R. Plais, L. Lavnevich, G. Muller, C. Villafuerte, G. Clavier, E. Quesnel, B. Racine, S. Meunier-Della-Gatta, J. P. Dognon, P. Thuéry, J. Crassous, L. Favereau and G. Pieters, *Adv. Funct. Mater.*, 2020, **30**, 2004838.
70 Y. J. Kong, Z. P. Yan, S. Li, H. F. Su, K. Li, Y. X. Zheng and S. Q. Zang, *Angew. Chem., Int. Ed.*, 2020, **59**, 5336–5340.
71 M. M. Zhang, X. Y. Dong, Z. Y. Wang, H. Y. Li, S. J. Li, X. Zhao and S. Q. Zang, *Angew. Chem., Int. Ed.*, 2020, **59**, 10052–10058.
72 T. Ikeda, M. Takayama, J. Kumar, T. Kawai and T. Haino, *Dalton Trans.*, 2015, **44**, 13156–13162.
73 T. Ikeda, K. Hirano and T. Haino, *Mater. Chem. Front.*, 2018, **2**, 468–474.
74 W. Chen, G. Qing and T. Sun, *Chem. Commun.*, 2016, **53**, 447–450.
75 W. J. Li, Q. Gu, X. Q. Wang, D. Y. Zhang, Y. T. Wang, X. He, W. Wang and H. B. Yang, *Angew. Chem., Int. Ed.*, 2021, **60**, 9507–9515.
76 H. Shang, Z. Ding, Y. Shen, B. Yang, M. Liu and S. Jiang, *Chem. Sci.*, 2020, **11**, 2169–2174.
77 D.-M. Li and Y.-S. Zheng, *J. Org. Chem.*, 2011, **76**, 1100–1108.
78 Y.-S. Zheng and Y.-J. Hu, *J. Org. Chem.*, 2009, **74**, 5660–5663.
79 J.-B. Xiong, H.-T. Feng, J.-P. Sun, W.-Z. Xie, D. Yang, M. Liu and Y.-S. Zheng, *J. Am. Chem. Soc.*, 2016, **138**, 11469–11472.
80 Y.-X. Yuan, M. Hu, K.-R. Zhang, T.-T. Zhou, S. Wang, M. Liu and Y.-S. Zheng, *Mater. Horiz.*, 2020, **7**, 3209–3216.
81 H. Qu, Y. Wang, Z. Li, X. Wang, H. Fang, Z. Tian and X. Cao, *J. Am. Chem. Soc.*, 2017, **139**, 18142–18145.
82 H.-T. Feng, X. Zheng, X. Gu, M. Chen, J. W. Y. Lam, X. Huang and B. Z. Tang, *Chem. Mater.*, 2018, **30**, 1285–1290.
83 D. D. L. Anuradha, M. Al Kobaisi, A. Gupta and S. V. Bhosale, *Chem.–Eur. J.*, 2017, **23**, 3950–3956.
84 D. D. L. Anuradha, M. Al Kobaisi and S. V. Bhosale, *Sci. Rep.*, 2015, **5**, 15652.
85 W.-G. Qiao, J.-B. Xiong, Y.-X. Yuan, H.-C. Zhang, D. Yang, M. Liu and Y.-S. Zheng, *J. Mater. Chem. C*, 2018, **6**, 3427–3434.
86 W. Shang, X. Zhu, T. Liang, C. Du, L. Hu, T. Li and M. Liu, *Angew. Chem., Int. Ed.*, 2020, **59**, 12811–12816.
87 D. Zhao, H. He, X. Gu, L. Guo, K. S. Wong, J. W. Y. Lam and B. Z. Tang, *Adv. Opt. Mater.*, 2016, **4**, 534–539.
88 M. Han, S. J. Cho, Y. Norikane, M. Shimizu and T. Seki, *Chem.–Eur. J.*, 2016, **22**, 3971–3975.
89 R. Eelkema and B. L. Feringa, *Org. Biomol. Chem.*, 2006, **4**, 3729–3745.
90 H. Goto and K. Akagi, *Angew. Chem., Int. Ed.*, 2005, **117**, 4396–4402.
91 B. A. San Jose, J. Yan and K. Akagi, *Angew. Chem., Int. Ed.*, 2014, **53**, 10641–10644.
92 E. M. Sanchez-Carnerero, A. R. Agarrabeitia, F. Moreno, B. L. Maroto, G. Muller, M. J. Ortiz and S. de la Moya, *Chem.–Eur. J.*, 2015, **21**, 13488–13500.
93 R. Carr, N. H. Evans and D. Parker, *Chem. Soc. Rev.*, 2012, **41**, 7673–7686.
94 H. Li, B. S. Li and B. Z. Tang, *Chem.–Asian J.*, 2019, **14**, 674–688.
95 A. Nitti and D. Pasini, *Adv. Mater.*, 2020, **32**, 1908021.
96 J. Kumar, T. Nakashima and T. Kawai, *J. Phys. Chem. Lett.*, 2015, **6**, 3445–3452.
97 Y. Wang, X. Li, F. Li, W. Y. Sun, C. Zhu and Y. Cheng, *Chem. Commun.*, 2017, **53**, 7505–7508.
98 N. L. Leung, N. Xie, W. Yuan, Y. Liu, Q. Wu, Q. Peng, Q. Miao, J. W. Lam and B. Z. Tang, *Chem.–Eur. J.*, 2014, **20**, 15349–15353.
99 J. Mei, Y. Hong, J. W. Lam, A. Qin, Y. Tang and B. Z. Tang, *Adv. Mater.*, 2014, **26**, 5429–5479.
100 D. W. Zhang, M. Li and C. F. Chen, *Chem. Soc. Rev.*, 2020, **49**, 1331–1343.